TAMPEREEN TEKNILLINEN YLIOPISTO
TAMPERE UNIVERSITY OF TECHNOLOGY

Ali H. Hanoon Al-Subi

Photoinduced Electron Transfer in Porphyrin- and Phthalocyanine-Fullerene Dyads in Non-Coordinating and Halide-Coordinating Environments

Julkaisu 1135 • Publication 1135

Tampere 2013

Tampereen teknillinen yliopisto. Julkaisu 1135
Tampere University of Technology. Publication 1135

Ali H. Hanoon Al-Subi

Photoinduced Electron Transfer in Porphyrin- and Phthalocyanine-Fullerene Dyads in Non-Coordinating and Halide-Coordinating Environments

Thesis for the degree of Doctor of Science in Technology to be presented with due permission for public examination and criticism in Festia Building, Auditorium Pieni Sali 1, at Tampere University of Technology, on the 31st of May 2013, at 12 noon.

Tampereen teknillinen yliopisto - Tampere University of Technology
Tampere 2013

ISBN 978-952-15-3077-7 (printed)
ISBN 978-952-15-3104-0 (PDF)
ISSN 1459-2045

Abstract

Photoinduced electron transfer (ET) in dyads consisting of zinc porphyrins or zinc phthalocyanines as the electron donors and fullerene C_{60} as the electron acceptor was studied in different environments. Time-resolved absorption and emission spectroscopy studies were performed to monitor the populations of the transient states involved in the ET reaction. In porphyrin-fullerene dyads the reaction proceeds via an intramolecular exiplex intermediate. The precursor of this state can be observed as a broad absorption band, also known as charge transfer (CT) band, in the far red part of the spectrum. The molar absorption of the CT band was strong enough to populate the intramolecular exciplex directly from the ground state by exciting the dyad at its CT band. By using this strategy the number of intermediate states in the excitation relaxation process was reduced to two, and the quantitative analysis of the ET reactions involving the exciplex and the complete charge-separated (CS) state was carried out by constructing a kinetic model based on the Marcus theory of ET and Boltzmann distribution law. The model was successfully applied to a zinc porphyrin-fullerene dyad and it allowed to evaluate the ET parameters, e.g. the free and reorganization energies, the electronic couplings for the exciplex and the complete CS state, and the charge separation degree in the exciplex. The developed model can be applied for such dyads at any value of the dielectric constant of the solvent.

Chloride binding to the central zinc of a zinc porphyrin-fullerene dyad results in drastic changes in the energies and lifetimes of the locally excited singlet state of porphyrin, the exciplex, and the complete CS state. The effects of the chloride coordination on the energies and lifetimes of the ET intermediates were examined and explained by the electric field effect on the donor chromophore induced by the negative charge of the chloride ion ligated to the central metal of porphyrin. The ligation results also in an increase of the oscillator strength of the CT absorption band.

Compared to porphyrin-fullerene dyads the chloride binding effect was found to be much weaker in zinc phthalocyanine-fullerene dyads. The forward ET reaction in the zinc phthalocyanine-fullerene dyads was found to occur in the Marcus inverted region. The latter conclusion was made because the chloride ligation to the zinc phthalocyanine moiety of the dyad was found to result in (i) an increase in the driving force of the ET reaction and (ii) a decrease in the ET rate constant.

Acknowledgements

The research work of this Thesis was carried out during the years 2009-2013 in the Department of Chemistry and Bioengineering at Tampere University of Technology. The Academy of Finland is acknowledged for the financial support of the research. I would like to thank also the Iraqi Ministry of Higher Education and Scientific Research, for covering my PhD studies in Finland.

Before I move to Finland, coming from Iraq with my family, Prof. Helge Lemmetyinen, my first supervisor, has done a lot of efforts to help me get the admission in Tampere University of Technology. It lasted more than one year, to carry out the formalities and leaving Iraq, until I joined his diverse research group in Tampere. Helge provided help throughout my research by motivating me to work, teaching me the theoretical aspects, and publishing the articles. I am deeply grateful to Helge for giving me this opportunity, which made it possible to do the PhD research under his supervision and also for his advices in my social life. On behalf of my family, I send Helge warm gratitude for all of his support in Finland.

My second supervisor, Prof. Nikolai Tkachenko, deserves my sincere gratitude for the enormous help he provided during my research time in the university. Nikolai was the first person I met after arriving Tampere as he picked me up with my family from the city center to my apartment in Hervanta. Nikolai has made the greatest role in my spectroscopy learning and understanding in both the theoretical and experimental parts of the work. He has done huge efforts in helping me gain the practical skills and overcome all the problems I faced during my research time.

I would like to thank warmly Dr. Marja Niemi for her contribution in the published articles and her important notes and suggestions on the Thesis. Marja has been always the person, who gives significant improvements to the scientific text in order to make it a high level and productive document.

I also acknowledge Dr. Alexander Efimov for all the “used compounds”, which were synthesized in the synthetic chemistry team and for his valuable advices and suggestions. My thanks go to the co-authors of the articles for supporting me during the way. Dr. Vladimir Chukharev owes my acknowledgement for his help in the explanation and use of various instruments in the lab.

For the pleasant work atmosphere throughout the research years, I am grateful to all my colleagues in the “Supramolecular Photochemistry group”. Especially I want to thank my friend Dr. Alexey Veselov for the nice time we shared away from research, and my classmates in the work office Rajeev Dubey, Tatu Kumpulainen, Dr. Somnath Dey, and Dr. Antti Tolkki, for providing an excellent ambience in the office.

I want to thank the Coordinator of International Affairs in Tampere University of Technology, MSc. Ulla Siltaloppi, for all the help provided to me and my family regarding the formalities and social affairs in Finland.

This work would not exist without the support from my wife, Amal, who has been standing by me and motivating me during the four years of the research. She made me believe, that I can overcome all the problems and finish the work successfully. I am very grateful to her for the dedication and all the help I received in my social and academic life. I will not forget to thank my beloved children, Hasan, Sara, and Ibrahim, for the relaxation and joy they brought into my life during my residence in Finland.

My gratitude cannot be complete without mentioning my dears in Iraq, my mother, brothers, and sisters. I am very grateful to them for all the support and encouragement I got throughout my studies and work in the university.

Tampere, May 2013

Ali Al-Subi

TABLE OF CONTENTS

List of publications

The Thesis is based on the following papers, which will hereafter be referred to by their Roman numerals:

I. Effect of Anion Ligation on Electron Transfer of Double-Linked Zinc Porphyrin-Fullerene Dyad

Ali H. Al-Subi, Marja Niemi, Nikolai V. Tkachenko, and Helge Lemmetyinen

J. Phys. Chem. A **2011**, *115*, 3263-3271.

II. Effect of Halide Binding on Intramolecular Exciplex of Double-Linked Zinc Porphyrin-Fullerene Dyad

Ali H. Al-Subi, Marja Niemi, Jenni Ranta, Nikolai V. Tkachenko, and Helge Lemmetyinen

Chem. Phys. Lett. **2012**, *531*, 164-168.

III. Quantitative Analysis of Intramolecular Exciplex and Electron Transfer in a Double-Linked Zinc Porphyrin-Fullerene Dyad

Ali Hanoon Al-Subi, Marja Niemi, Nikolai V. Tkachenko, and Helge Lemmetyinen

J. Phys. Chem. A **2012**, *116*, 9653-9661.

IV. Effect of Anion Coordination on Electron Transfer in Double-Linked Zinc Phthalocyanine-Fullerene Dyad

Ali Hanoon Al-Subi, Alexander Efimov, Marja Niemi, Nikolai V. Tkachenko, and Helge Lemmetyinen

Chem. Phys. Lett., article in press

DOI information: http://dx.doi.org/10.1016/j.cplett.2013.04.035

Abbreviations and symbols

a	free energy coefficient
a_i	pre-exponential factors
A	acceptor
A	absorbance
A_0	frequency independent constant
ΔA	absorption change
b_{cs}	reorganization energy coefficient of complete CS state
b_{ex}	reorganization energy coefficient of exciplex
$[cs]$	population of complete CS state
C_0	frequency independent scaling factor
C_{60}-ref	fullerene reference compound
CT	charge transfer
CCD	charge-coupled device
CFD	constant fraction discriminator
CS	charge separation, charge-separated
CR	charge recombination
D	donor
DA	donor-acceptor pair
D^*A	locally excited state of donor
DA^*	locally excited state of acceptor
$D^{\bullet+}A^{\bullet-}$	complete CS state
$(DA)^*$	exciplex state

DAS	decay associated spectra
DCB	ortho-dichlorobenzene
DHD6ee	61,62-diethyl[10,20-bis(3-(2-hydroxyethoxy)-phenyl)porphyrin-5,15-diylbis(1-phenyl-3-oxy)-diethylene]1,9:49,59-bismethano[60]fullerene-61,61,62,62-tetracarboxylate
DMF	dimethyl formamide
DPV	differential pulse voltammetry
eV	electron volt
$[ex]$	population of exciplex state
E_0	solvent independent part of free energy
E_A	activation energy
E_{ox}	oxidation potential of donor moiety in DA pair
E_{ph}	energy of phthalocyanine first singlet excited state
E_{red}	reduction potential of acceptor moiety in DA pair
E_v	energy of vibrational mode
ET	electron transfer
f_s	solvent polarity factor
f	oscillator strength
F	model decay function
FWHM	full width at half-maximum
ΔG°	Gibbs free energy change
ΔG_{cs}	free energy of complete CS state
$-\Delta G_{CS}$	driving force of CS process
ΔG_{ex}	free energy of exciplex
h	Planck's constant

i	vibrational level
I	emission intensity or electric current
IR	infrared
k_B	Boltzmann's constant
k_{cx}	rate constant of back reaction from complete CS state to exciplex
k_{CR}	rate constant of charge recombination process
k_{CS}	rate constant of charge separation process
k_{ET}	rate constant of electron transfer from reactant to product
k_{ex}	relaxation rate constant of exciplex to ground state
k_{exp}	experimental rate constant
k_{fit}	calculated common rate constant for exciplex and complete CS state
MCA	multichannel analyzer
n	refractive index of medium
NLC	non-linear crystal
PD	photodetector
PhCN	benzonitrile
PMT	photomultiplier tube
q_e	elementary charge
R_A	acceptor radius
R_D	donor radius
R_{DA}	center-to-center distance between donor and acceptor
S	electron-vibrational coupling
S_1	first electronic singlet excited state
SHG	second harmonic generator

t	time
T	temperature
$TBABF_4$	tetra-*n*-butylammonium tetrafluoroborate
TBACl	tetra-*n*-butylammonium chloride
$TBAPF_6$	tetra-*n*-butylammonium hexafluorophosphate
TBD6be	6162-di-*tert*-butyl-61,62-[10,20-bis(3,5-di-*tert*-butylphenyl)porphyrin-5,15-diylbis(1-phenyl-3-oxy)-diethylene]1,9:49,59-bismethano[60]fullerene-61,61,62,62-tetracarboxylate
TAC	time-to-amplitude convertor
TCSPC	time-correlated single photon counting
UV	ultraviolet
V	electronic coupling matrix element between reactant and product
ZnP	zinc porphyrin
ZnP-ref	zinc porphyrin reference compound
ZnPc	zinc phthalocyanine
ZnDHD6ee	Zinc (II) complex of **DHD6ee**
ZnPc-C_{60}ee	Zinc (II) complex of double-linked phthalocyanine-fullerene dyad
ZnTBD6be	Zinc (II) complex of **TBD6be**
β_{cs}	relative population of exciplex
β_{ex}	relative population of complete CS state
γ	charge separation degree
ε	molar absorption coefficient
ε_0	permittivity of vacuum
ε_r	static dielectric constant
κ_{el}	electronic transmission coefficient

λ	wavelength
λ_r	total reorganization energy
λ_{ri}	inner reorganization energy
λ_{rs}	solvent (outer) reorganization energy
ν	frequency or wave number
ν_n	frequency of passage through transition state
$\Delta\nu$	bandwidth
σ^2	mean square deviation
τ	lifetime of transient state
Ψ	wave function

1 Introduction

The electron transfer (ET) is an essential phenomenon for many fields of chemistry and also for many biological redox processes that are crucial for life, such as metabolism and photosynthesis. For example, in natural photosynthetic membranes, arrays of chlorophyll molecules are used as antennas to capture sunlight and the collected energy is transferred to a reaction center, where it is utilized in the ET reaction generating an electrostatic potential energy between two chromophores [1-5]. Then, this electrostatic potential energy is used in the production of adenosine tri-phosphate, the energy currency of living organisms.

Mimicking the charge separation occurring in the reaction centers of natural photosynthesis is a very challenging task because of the complexity of this process. Therefore, the design of artificial models of the photosynthetic centers becomes necessary to achieve the ET reaction in molecular systems [5-10]. Recently, more efforts have been devoted to the design and synthesis of molecular and/or supramolecular species that can function as antennas and reaction centers in artificial systems for the photochemical conversion of solar energy. The simplest mimic can be a dyad molecule consisting of an electron donor (D) and an electron acceptor (A), which represents a donor-acceptor pair (DA) with at least one of the species being capable to absorb the light [2,4].

The combination of porphyrins and/or their analogues phthalocyanines with fullerenes can serve as efficient DA systems [5,8,11-14]. The ET reactions of porphyrin- and phthalocyanine-fullerene DA compounds have remarkably small reorganization energies, which arise from the large π electron systems delocalized over the porphyrin and/or phthalocyanine surface together with the confined structure of the aromatic fullerene spheroid [15-17]. The porphyrin- and phthalocyanine-fullerene compounds are promising structures for designing organic solar cells and other molecular electronic systems. The outstanding property of porphyrin-fullerene DA dyads is their ability to undergo fast photoinduced ET and slow charge recombination (CR), thus generating a long-lived charge separated (CS) state, which fulfills the requirements for an efficient photosynthetic reaction center [5,8,11,13]. In addition, it has been reported that phthalocyanine-fullerene dyads undergo photoinduced ET even in non-polar media, e.g. in toluene, as well as in polar solvents [18]. One of the important factors that control the ET

reaction is the center-to-center distance between the donor and acceptor. Two covalent linkers with a suitable length can be an effective approach to build up a dyad with D and A brought in close contact to achieve a symmetric structure with face-to-face orientation [12,19-23].

In addition to the center-to-center distance between D and A species, the environment has a significant impact on the ET mechanism of such DA compounds. Specifically, the presence of ligands in the solution of the dyad molecules gives the opportunity to build new chemical systems where the ligand binds with the central metal of the donor moiety, e.g. the zinc pophyrin or the zinc phthalocyanine. The new coordination bond between the central metal and the ligand can result in a considerable change in the ET reaction properties of the dyad [13,24]. The electric field, induced by the ligand, around the dyad molecule leads to a change in the energies of the intermediates involved in the photoinduced ET reaction, which in turn affects the rate of the charge separation and recombination processes.

The optimization of systems capable of ET requires that the reaction mechanisms are known in detail. The first step is the study of the intramolecular reactions of the DA compounds in solutions. Such studies necessitate the use of time-resolved spectroscopy techniques and advanced theoretical methods to analyze the experimental results. This Thesis aims to offer a contribution to the understanding of the photoinduced ET phenomenon in zinc pophyrin- and zinc phthalocyanine-fullerene dyads taking place in solvents with different polarities as well as in ionic environments, i.e. in the presence of strong negatively charged ligands such as chloride or bromide ions. In addition, special attention was paid to the intramolecular exciplex of the zinc porphyrin-fullerene dyads, which is a common and important intermediate in the photoinduced reactions of such dyads.

All the dyads under study have two covalent linkers to restrict the conformational freedom of the donor and acceptor chromophores by keeping them at a fixed orientation. In order to gain information on the equilibrium reaction between the exciplex and the complete CS state in porphyrin-fullerene dyads, a theoretical model was constructed to achieve a clear quantitative discrimination between the exciplex and the complete CS state even though their transient absorption spectra are rather similar [III]. The studies published in papers [I,II,IV] are devoted to understand the role of the halide binding to the zinc porphyrin- and zinc phthalocyanine moieties of the dyads in the ET reaction schemes and the exciplex properties.

2 Background

2.1 Marcus theory for electron transfer

For the design of artificial molecular systems, it is essential to understand the principles of the processes occurring in the natural photosynthetic reaction centers and the factors that make these reactions possible. A qualitative understanding of the theoretical background behind the ET reactions can be gained from the classical Marcus theory [25-29]. In a system consisting of an electron donor (D) and an electron acceptor (A), an ET takes place from D to A, resulting in the generation of a CS state ($D^{\bullet+}A^{\bullet-}$). In the ET processes, D and A can be either two separate molecules, or two moieties of the same molecule. The former and the latter are usually referred to as the intermolecular and the intramolecular ET reactions, respectively. In the photoinduced ET reactions of simple conjugates the reactant (the initial state) is a locally excited state of either the donor ($D^{*}A$) or the acceptor (DA^{*}) generated from the ground state (DA) by a photo-excitation process, and the product (the final state) is the complete CS state ($D^{\bullet+}A^{\bullet-}$). The Marcus theory of ET succeeds also to interpret the charge recombination process, i.e. the transition from the CS state to the ground state in addition to the forward ET reaction.

According to this theory, the multidimensional potential energy surface connecting the reactant and product states is reduced to a single dependence on so-called generalized reaction coordinate with parabolic dependences in vicinities of the reactant and product equilibrium states (Figure 2.1) [25-28]. The reaction coordinate describes the changes in the nuclear coordinates of the molecule itself and in those of the surrounding solvent molecules.

In the classic ET theory the curvatures of both the reactant and product state potentials are assumed to be the same [26]. Therefore, the surface of the product state is resulted from shifting the parabola of the reactant surface in both axes, i.e. in the energy and reaction coordinate scales. At a point where both the reactant and product states have similar nuclear coordinate configuration the ET reaction occurs. This means that the ET reaction proceeds at the transition state where the reactant and product parabolas intersect each other (Figure 2.1). The difference between the minimum energy of the reactant state and the energy where both reactant and product surfaces intersect is called the activation energy, E_A, of the ET reaction (Figure 2.1).

Therefore, the reactant state undergoes ET only when its surface potential distorts from the equilibrium by E_A [26,29].

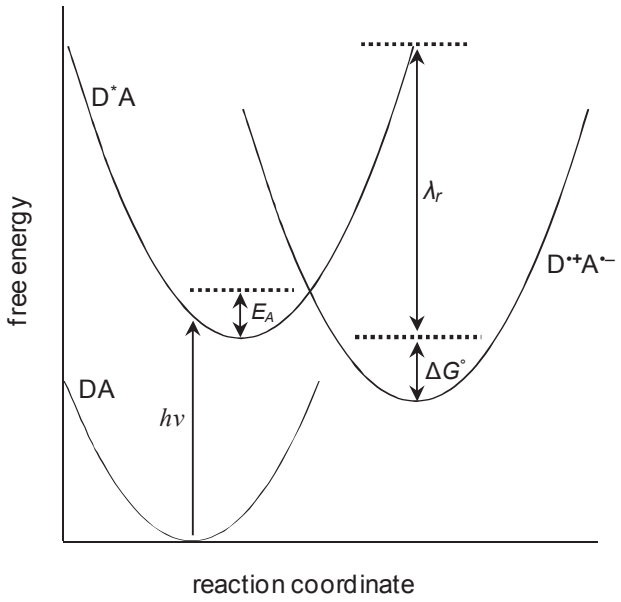

Figure 2.1 Potential energy surfaces for the ground state (DA), the excited state (D^*A, reactant state), and the complete CS state ($D^{\bullet+}A^{\bullet-}$, product state) versus the reaction coordinate. The initial step is photo-excitation of the DA system to the excited state via a vertical transition.

The ET rate constant, k_{ET}, can be obtained from the classical transition state theory where the population of the transient state follows the Boltzmann distribution law [25,26]:

$$k_{ET} = \kappa_{el} \nu_n \exp\left[-\frac{E_A}{k_B T}\right], \tag{2.1}$$

where κ_{el} is the electronic transmission coefficient or probability to change the parabola, ν_n is the frequency of passage (nuclear motion) through the transition state, which has a value close to the vibrational frequency, 10^{13} s^{-1} [26], k_B is Boltzmann's constant, and T is the temperature. Within the parabolic approximation of the potential energy curves, the activation barrier for the ET reaction is expressed as:

$$E_A = \left[\frac{(\Delta G^0 + \lambda_r)^2}{4\lambda_r}\right], \tag{2.2}$$

where ΔG° is the change in Gibbs free energy for the ET reaction, and λ_r is the total reorganization energy. The reorganization energy represents the change in Gibbs energy if the reactant state were to distort to the equilibrium configuration of the product state without transfer of the electron. Thus, the classical expression for the ET rate constant is [26]:

$$k_{ET} = \kappa_{el} \nu_n \exp\left[-\frac{(\Delta G^0 + \lambda_r)^2}{4\lambda_r k_B T} \right]. \quad (2.3)$$

The Gibbs free energy with negative sign, $-\Delta G^{\circ}$ in Equation 2.3, is called the driving force of the ET reaction. In the classical Marcus theory of ET (Equation 2.3), there is an interesting feature because the driving force of the ET reaction determines the activation energy for a fixed value of the reorganization energy and as a result determines the rate of the ET reaction. If $-\Delta G^{\circ} < \lambda_r$, an increase in the driving force of the ET reaction results in a decrease in the activation energy barrier and therefore in an increase in k_{ET}. This regime is called the normal region, because the reaction becomes more exergonic with increasing the driving force. When $-\Delta G^{\circ} = \lambda_r$, the maximum ET rate is achieved. When the driving force of the ET reaction becomes larger than the reorganization energy, $-\Delta G^{\circ} > \lambda_r$, the barrier of the activation energy reappear again and the rate of the ET reaction is slowed down, which is called the Marcus inverted region [25-29].

The reorganization energy is usually divided into two terms, the internal component term, λ_{ri}, and the outer sphere or the solvent reorganization energy, λ_{rs}, as follows [26,28]:

$$\lambda_r = \lambda_{ri} + \lambda_{rs}. \quad (2.4)$$

The internal component arises from the structural differences between the equilibrium configurations of the reactant and product states and it is expected to be quite small particularly for the molecules having big and highly symmetrical structure. The outer term arises from differences between the orientation and polarization of solvent molecules around the reactant and product states of the studied system [26].

According to the classic dielectric continuum model [26,28], the dependence of the solvent reorganization energy on the medium polarity is predicted to be:

$$\lambda_{rs} = b f_s = b\,(1/n^2 - 1/\varepsilon_r), \quad (2.5)$$

where f_s is the solvent polarity factor, n is the refractive index of the medium, and ε_r is the dielectric constant of the solvent. The parameter b is a coefficient in the linear dependence of λ_{rs} on f_s.

The coefficient b has been defined according to the spherical approximation of the donor and acceptor as follows [26,28,30,31]:

$$b = \frac{q_e^2}{4\pi\varepsilon_0}\left[\frac{1}{2R_D} + \frac{1}{2R_A} - \frac{1}{R_{DA}}\right], \tag{2.6}$$

where q_e is the elementary charge, ε_0 is the permittivity of vacuum, R_D and R_A are the radii of the donor and acceptor, R_{DA} is the center-to-center distance between the donor and acceptor.

The Marcus theory of ET is applied successfully for mono-step ET reactions explained above. However, when the ET reaction proceeds via an intermediate the quantitative analysis using one-dimensional model becomes difficult [32]. One example is the presence of the exciplex as an intermediate in the ET reaction, which will be explained in the following section.

Equation (2.3) works reasonably well for so-called adiabatic ET, when $\kappa_{el} \approx 1$ and the system remains on a single potential energy surface. For diabatic or non-adiabatic ET reactions a quantum mechanical treatment becomes necessary. This treatment considers the probabilities of the electronic and nuclear tunneling between the reactant and product states. The expression for the quantum mechanical calculations of ET rate is [25-27,29]:

$$k_{ET} = \frac{2\pi^{3/2}V^2 e^{-S}}{h(\lambda_r k_B T)^{1/2}} \sum_{i=0}^{\infty} \frac{S^i}{i!} \exp\left[-\frac{(\Delta G^0 + \lambda_r + iE_v)^2}{4\lambda_r k_B T}\right], \tag{2.7}$$

where V is the electronic coupling matrix element between the reactant and product, S is the electron-vibrational coupling, h is Planck's constant, i is the vibrational level, and E_v is the energy of the vibrational mode.

A more careful consideration for the pre-exponential factor in the classical theory of ET (Equation 2.3) is obtained from the comparison with the semi-quantum treatment (Equation 2.7). This gives the dependence of the ET rate constant on the electronic coupling as follows [25-29]:

$$k_{ET} = \frac{2\pi^{3/2}V^2}{h(\lambda_r k_B T)^{1/2}} \exp\left[-\frac{(\Delta G^0 + \lambda_r)^2}{4\lambda_r k_B T}\right], \quad (2.8)$$

where ΔG^0 is the Gibbs free energy of the ET process, i.e. the driving force of the reaction.

2.2 Exciplex and charge-transfer absorption and emission bands

The definition of an exciplex according to IUPAC is an electronically excited complex, of definite stoichiometry, "non-bonding" in the ground state [33]. For example, the exciplex can be a complex formed by the interaction of an electronically excited molecular entity with a ground state partner of a different structure. The terms "compact exciplex" and "loose exciplex" have sometimes been used to indicate that such exciplexes may have structures closely related to a contact ion pair or a solvent-separated ion pair [33].

In some conditions, when the interaction between the donor and the acceptor is strong, the exciplex can be formed and it may have sufficiently long lifetime to undergo light emission [34-36]. This emission is a distinctive quality for the exciplex and it is usually used to characterize the exciplex state, where the emission band appears as a broad band in the red and near IR spectral regions [34-36]. The exciplex state can also be characterized by a partial shift of electron density from the donor to the acceptor, and a large dipole moment, which reflects the degree of the charge transfer [37-39].

Since the two distinct properties of the exciplexes are the charge shift and the electronically excited state, the term CT complex is sometimes used as an alternate name to the term exciplex. In fact, the terms exciplex and excited CT complex have been used to describe such excited CT states, where the donor and acceptor do not form a complex in the ground state, and excited state charge transfer occurs upon bimolecular encounter of an excited molecule and a quencher [37-39]. An excited CT complex, however, can be formed either as a result of a bimolecular quenching reaction, or directly by light absorption in the CT band of the ground state complex.

It has been found that even in relatively simple DA conjugates, the photoinduced inter- and intramolecular ET reactions can be complex and multi-step processes, when the exciplex is formed as an intermediate [34-40]. Under certain conditions the exciplex lowers the potential

energy barrier between the locally excited state and the complete CS state, and thus accelerates the ET process [23,41-44].

The environment affects the exciplex properties significantly. When the exciplex is formed as an intermediate in the ET reaction prior to the generation of the complete CS state, the lifetime, the energy, and the emission quantum yield of the exciplex decrease with the increase of the solvent polarity [34,40,45]. The free energy of the exciplex (ΔG_{ex}) has been found to depend linearly on the inverse of the dielectric constant of the solvent as follows [31]:

$$\Delta G_{ex} = E_0 + \left[\frac{a}{\varepsilon_r}\right], \tag{2.9}$$

where E_0 is a constant representing the free energy of the exciplex when the Coulombic attraction between the donor and acceptor is neglected and a is a coefficient showing how strong is the dependence.

According to the simple point-to-point interaction model and assuming that the only solvent-sensitive part of the free energy of the exciplex (and also of the complete CS state) is the Coulombic interaction between the donor and the acceptor, the coefficient a in Equation 2.9 will have the same expression as the coefficient b given in Equation (2.6). This means that a is the solvent independent coefficient, which depends only on the molecular structure [25,26,28-31] (see Section 2.1).

The case of the porphyrin-fullerene systems is unique in the sense that the energies of the locally excited states of both porphyrin and fullerene chromophores, and the energy of the complete CS state are relatively close to each other, which facilitates the formation of the exciplex intermediate in the ET reaction. Although the exciplex intermediate is highly probable in such ET reactions, its experimental observation and quantitative characterization are challenging tasks. The reason for this is that the exciplex has features of both its precursor and product, the locally excited state and the complete CS state, respectively, being not easily distinguishable in transient absorption measurements. As stated above, the most characteristic quality of the exciplex is its distinctive emission band in the red and the near IR spectral regions, which has been detected for many non-bonded and covalently bonded DA systems particularly in non-polar environments [23,27,35-37,39-41,43-45].

Detailed photophysical investigations of the covalently linked porphyrin-fullerene DA compounds have revealed spectroscopic and kinetic evidence, which suggest that the ET reaction occurs via an intramolecular exciplex [12,41,42,46]. It has been demonstrated that the complete CS state is not observed for a series of porphyrin-fullerene dyads in non-polar solvents because its energy has been found to be higher than that of the exciplex [12,41]. Instead, in non-polar solvents, the characteristic exciplex emission in the red and near IR spectral regions has been seen particularly for the dyads, which have a face-to-face orientation between the donor and acceptor [12,46,47-50].

The photodynamics of the exciplex formation and decay depend strongly on the distance and mutual orientation between the donor and acceptor [12,46-48,50]. The covalently linked porphyrin-fullerene dyads with short center-to-center distance between the porphyrin and fullerene moieties present a unique DA system [12,19,20,46,47,51], because they may provide a pre-formed intramolecular complex. Unlike for many other DA systems where the exciplex is formed only after excitation of one of the chromophores, in such porphyrin-fullerene dyads the intramolecular exciplex is characterized by a relatively strong CT absorption band, which is observed in the red-near IR spectral region [12,31,41,46-50]. For such porphyrin-fullerene dyads, the energetic parameters associated with the exciplex can be obtained by analyzing the steady state CT absorption and emission bands in frame of the semi-quantum electron transfer theory [27,31,38,39,49,52]. These parameters are: the free, vibrational, and reorganization energies, the electron-vibrational coupling, and the electronic coupling matrix element.

According to the Marcus ET theory, the shape of the CT emission band is presented as a weighted sum of Gaussians [27,31,38,39,48,52]:

$$I(\nu) = C_0 \sum_{i=0}^{\infty} \frac{S^i}{i!} \exp\left[-\frac{(\Delta G^\circ - \lambda_{rs} - iE_v - h\nu)^2}{4\lambda_{rs} k_B T} \right], \tag{2.10}$$

where ν is the light frequency, ΔG° is the free energy, i.e. the exciplex energy relative to the ground state, and C_0 is a constant. The coefficient C_0 is a frequency independent scaling factor, which determines only the emission density [12,31]. Thus, the fit of an experimentally available CT emission to Equation 2.10 gives the energetic parameters associated with the exciplex, i.e. ΔG°, λ_{rs}, E_v, and S.

The spectrum shape of the CT absorption band can also be obtained from the Marcus theory, which gives the following equation [29,31,39,52]:

$$A(\nu) = A_0 \sum_{i=0}^{\infty} \frac{S^i}{i!} \exp\left[-\frac{(\Delta G^\circ + \lambda_{rs} + iE_v - h\nu)^2}{4\lambda_{rs} k_B T} \right], \tag{2.11}$$

where A_0 is the frequency independent constant [12,31]. In the case of porphyrin-fullerene systems, S is smaller than unity and the major components of the absorption and emission spectra originate from the transitions between states of zero vibrational levels, i.e. $i = 0$ [31,48,49], but a more reliable fitting can be achieved by taking into account for example six vibrational levels (i = 0-5) and neglecting only the transitions to higher vibrational modes [31].

It has been earlier reported that the CT emission band shifts to the red, becomes broader, and decreases in intensity upon increasing the solvent polarity [12,31,40,46-50]. These effects have been attributed to the increase in solvent reorganization energy and lowering of the exciplex energy in solvents with higher polarity.

The electronic coupling matrix element, V, (indicated in Equations 2.7 and 2.8) cannot be directly obtained from the CT absorption bands using the model given in Equation (2.11), because this parameter is included in the constant A_0, which is directly related to the transition dipole moment of the molecule [52]. Under certain simplifications, the electronic coupling can be evaluated from the center-to-center distance between the donor and acceptor, R_{DA}, and the spectrum shape and intensity as follows [12,29,48]:

$$V = \frac{2.06 \times 10^{-2}}{R_{DA}} (\varepsilon_{\max} \nu_{\max} \Delta\nu)^{1/2}, \tag{2.12}$$

where $\varepsilon_{\max}$ and $\nu_{\max}$ are the molar absorption coefficient ($M^{-1}cm^{-1}$) and the light frequency (cm^{-1}) at the maximum of the CT band, respectively, and $\Delta\nu$ is the bandwidth (cm^{-1}) of the CT absorption.

For the direct non-radiative relaxation of the exciplex to the ground state, it is possible to calculate the rate constant using the same formula derived for the ET reactions, i.e. Equation 2.7 [25-27,29]. In fact, the electronic coupling matrix element determines the magnitude of the non-radiative relaxation rate constant [25-27,29,39].

The magnitude of the electronic coupling between the donor and acceptor can be evaluated in frame of a suitable ET theory applied to the studied system, whether it is an adiabatic or a non-adiabatic reaction [25-27,29]. In non-adiabatic ET reactions, the electronic coupling between the donor and acceptor is small while in adiabatic processes the electronic coupling is large [25-27,29]. However, for the exciplex-ground state transitions, in some cases the non-adiabatic model can be valid even with strong electronic coupling between the states. It has been reported earlier that the electronic coupling for the exciplex can be a 100 times larger than that of the complete CS state in DA compounds of aromatic hydrocarbons [53]. This result can be explained by presenting the wave function of the exciplex, $\Psi_{(DA)^*}$, as a linear combination of the locally excited state wave function of the donor or acceptor, $\Psi_{(D^*A)}$ or $\Psi_{(DA^*)}$, and the complete CS state wave function, $\Psi_{(D^{\bullet+}A^{\bullet-})}$, and thus it is expected to have larger coupling with the ground state wave function than the complete CS state wave function alone [27,38,39,53]. In particular, the electronic coupling for the exciplex formed between a methyl benzene donor and a tetracyanoanthracenene acceptor has been reported to be ~0.17 eV [54]. The strong electronic coupling for the exciplex state has been deduced from a study of the quantitative relationship between the radiative and non-radiative electron transfer reactions [27,54,55]. Gould et al. have shown that the non-adiabatic and adiabatic theories are in quantitative agreement when the sum of the reorganization and vibrational energies is considerably smaller than the driving force of the ET reaction, i.e. $\Delta G_{ex} >> E_v + \lambda_r$ (Equation 2.7) for the direct relaxation of the exciplex to the ground state [27,55]. Instead, if ΔG_{ex} would approach $E_v + \lambda_r$, the adiabatic theory should be applied to this case [55].

Since the oscillator strength, f, of an electronic transition is directly proportional to the integral of the molar absorptivity of the absorbing molecule, the oscillator strength of the transition from the ground state to the exciplex state can be determined from the corresponding CT absorption spectrum using the following equation [56]:

$$f = 4.32 \times 10^{-9} Mcm^2 \int \varepsilon d\nu \,, \tag{2.13}$$

where ε is the molar absorption coefficient ($M^{-1}cm^{-1}$) and ν is the wave number (cm^{-1}). The calculation of the oscillator strength of an electronic transition helps to compare absorption bands belonging to the same transition but having different bandwidth, absorption intensity, and

wavelength position. The electronic coupling and the oscillator strength are two correlated parameters, i.e. higher electronic coupling leads to higher oscillator strength of the electronic transition and vice versa.

2.3 Porphyrins, phthalocyanines, fullerenes and their dyads

In the artificial models of photosynthetic reaction centers, porphyrins and their analogues phthalocyanines are often used as mimics of chlorophylls, since they belong to the same class of compounds and share similar electron and energy donating properties [5]. Porphyrin is a macrocyclic molecule that consists of a fundamental skeleton of four pyrrole rings connected at their alpha carbons via methane bridges [57]. The phthalocyanine macrocycle consists of four isoindole units, which are linked each other by aza bridges. The basic structural unit of porphyrin is named as porphine (Figure 2.2). The four pyrrole rings in porphyrins and phthalocyanines are connected so that the nitrogen atoms face inward. This structure forms a central cavity that can bind a wide variety of cations, including the transition metals which results in an alteration of many properties of the compounds [58]. Non-metallated porphyrins and phthalocyanines are known as free-base compounds. In addition, the properties of porphyrins can be changed by a chemical modification introducing different types of substituents onto the peripheral positions of the macrocycles. This modification alters for example the solubility, the redox potentials, and the electronic spectra, which in turn alters the donating ability of these chromophores in the photoinduced processes.

Porphyrins have high absorptivity at the blue part of the spectrum. The highly conjugated aromatic macrocyclic structure results in an intensive absorption ($\varepsilon > 2 \times 10^5$ $M^{-1}cm^{-1}$) at approximately 410-435 nm in the UV-visible absorption spectrum [59,60]. This absorption maximum is termed as the Soret band [57]. In addition, there are several weaker absorption maxima in the range 450-700 nm, which are called Q bands. The free-base porphyrin exhibits four Q bands whereas the metallated porphyrin shows only two Q bands in the visible absorption spectrum. The Soret band corresponds to a transition from the electronic ground state to the second singlet excited state, while the Q bands originate from transitions to the first singlet excited state [61,62].

Compared to porphyrins, phthalocyanines have higher extended π electron aromatic system. These chromophores are thermally and chemically stable and absorb the light more intensively in the red-near IR region of the spectrum [58,63]. The Soret band for phthalocyanines is weaker while the Q band absorption is more intensive. In addition, the fluorescence quantum yields of phthalocyanines are higher than those of porphyrins, making them suitable for efficient light-harvesting antenna systems. Similarly to porphyrins, phthalocyanines are synthetically versatile compounds as the two hydrogen atoms of the central cavity can be replaced by more than 70 metals and a variety of substituents can be incorporated in their structure [64].

Fullerenes are molecules that consist solely of carbon atoms arranged to form a closed surface composed of 12 pentagons and a varying number of hexagons [65,66]. The most stable structure of fullerenes is the one consisting of 60 carbon atoms, i.e. C_{60} or buckminsterfullerene [66]. C_{60} is the smallest fullerene where all the pentagons are isolated from each other by hexagons (Figure 2.2). The C_{60} fullerene absorbs light in the UV region of the spectrum at shorter than 300 nm while it has only weak absorption in the visible region. The large number of carbon atoms arranged in highly symmetrical three-dimensional configuration of the C_{60} molecule results in its unique properties as an electron acceptor in DA compounds. It can accommodate up to six electrons in solution [67,68] and the reorganization energies of the C_{60} containing DA dyads are significantly lower compared to otherwise similar dyads with different acceptor moieties [15-17]. The term "fullerene" in the entire Thesis text refers to C_{60} because it was the lonely electron acceptor used in the present study.

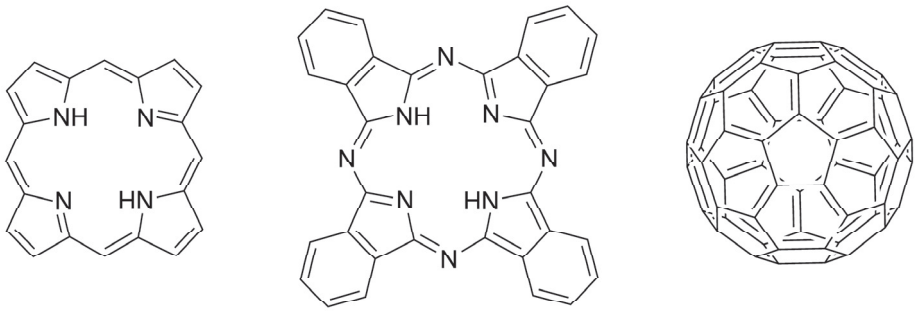

Figure 2.2. Structures of Porphine, Phthalocyanine, and C_{60} Fullerene.

Porphyrin-fullerene DA compounds can serve as models of the photosynthetic reaction center because they exhibit fast charge separation and slow charge recombination processes [8,9,15,16,20,24,69-73]. Since the absorptions of both porphyrin and phthalocyanine in the visible region are much stronger than that of fullerene, they are usually the chromophores being photo-excited in these systems. To achieve an efficient photoinduced ET in the above mentioned molecular assemblies, numerous attempts to model the optimal geometry of the dyad and to probe its impact on ET reactions have led to the development of a variety of porphyrin- and phthalocyanine-fullerene DA dyads, which give rise to different topologies and chromophore separations [5-14,17-23,41,46-50,63,64,69-74].

The highly efficient donating properties of phthalocyanines render them ideal molecular components in DA ensembles [18,58,63,64]. The phthalocyanine-fullerene dyads have a potential advantage over the porphyrin-fullerene dyads in possibility to undergo photoinduced ET even in non-polar media, e.g. in toluene, as well as in polar solvents [18].

As was shown in Section 2.1, the distance between the centers of the donor and acceptor, R_{DA}, affects the reorganization energy and as a result the rate of the ET reaction. Therefore, the porphyrin- and phthalocyanine-fullerene DA dyads, which have the face-to-face orientation between D and A and short R_{DA} has been found to undergo fast charge separation process because of the large interaction between D and A moieties [12,19-23]. Such orientation can be achieved by combining the two species of the dyad symmetrically with two molecular chains [12,19-23].

2.4 Ligand coordination effect on ET reactions

The naturally occurring metalloporphyrins, such as iron (II) porphyrins are essential to the human life as they play vital roles in the transport and storage of oxygen through the binding of molecular oxygen to the central iron (II) ion in the hemoglobin protein [75,76]. Similarly to processes taking place in nature, such binding plays an important role also in chemistry. As mentioned above, the existence of the central cavity in the synthetic free-base porphyrin and phthalocyanine macrocycles (Figure 2.2) enables the metallation with a wide variety of cations, including the transition metals [58]. In addition, the axial ligand binding to the zinc porphyrin and zinc phthalocyanine can give a rise to various extended supramolecular systems [13,24].

In the studies of metalloporphyrin complexes, e.g. transition metal complexes, it has been observed that the paramagnetic electronic configuration of the metal rapidly deactivates the excited states of the compounds and makes the fluorescence lifetime very short [77]. Instead, the filled *d*-shell of zinc atom does not quench the porphyrin singlet excited state fluorescence [78-80], which makes the zinc (II) porphyrin complexes, together with free-base porphyrins ideal building blocks in the construction of synthetic light harvesting models [5,58,81-83]. Zinc porphyrin complexes provide simple systems among the wide variety of metalloporphyrins for the study of a range of different ligands that axially bind to the central zinc. This simple system is based on the electronic configuration of the zinc ion (d^{10}), which leaves only one coordination degree of freedom of the resulted complex, i.e. the four-coordinate zinc porphyrin macrocycle accepts only one axial ligand to form a five-coordinate complex [84-86]. The axial coordination of ligands to the central zinc has a strong effect on the energetics and the ET processes in metalloporphyrin-based DA compounds. The binding effect of nitrogenic ligands, such as amines, imidazoles, and pyridines, on the properties of metalloporphyrins and metalloporphyrin-fullerene DA assemblies has been extensively studied [13,24,69,85-89]. The effects ranged from minor to drastic changes in the energetic properties of the porphyrin chromophore and the rate constants of the photoinduced energy and ET reactions.

The main effect of the axial coordination of ligands to zinc porphyrin (ZnP) is the change in the energetic properties of the chromophore. It is well established that ligation of bases, including anions, to metalloporphyrins lowers the potential for one-electron oxidation of the porphyrin molecule. The effect of various anions on the electrochemistry of zinc tetraphenylporphyrin has been previously studied in dichloromethane, and it has been revealed that the difference in the first one-electron oxidation potentials between the non-ligated and fully chloride-ligated ZnP is about 0.35 eV [89]. The spectroscopic features of zinc porphyrins can also be altered by the binding: the entire absorption of the chromophore shifts to the red and the intensity ratio of the low to high energy Q bands increases upon the binding of ligands to the central zinc [87,89,90]. However, Seely and Nappa have shown that the effects of the ligand on the ZnP properties depend on its charge and polarizability and not on the strength of the Zn-ligand bond, i.e. the negatively charged ligands have stronger effects than the neutral ones and thus halides, such as the chloride ion, have been found to be the most effective ligands in tuning the energetic and

spectral properties of the ZnP chromophore [89,90]. Furthermore, the quantum yields of the ZnP cation radical formation in the ligand-assisted ET reaction from the triplet state of ZnP to 1,4-benzoquinone have been earlier studied using substituted pyridines and chloride ion [87]. The study demonstrated that the quantum yield of the formation depends on the ligand's ability to shift negative charge toward the porphyrin ring via the central zinc. The chloride ion has been found to be the most effective one among the investigated ligands on the stabilization of the ion pair, because it resulted in remarkable enhancement of the quantum yield of the complete CS state. Moreover, it has been reported that the binding of chloride ion to the terminal zinc (II) porphyrin of selectively metalated triad and tetrad porphyrin arrays allows controlling the photoinduced energy and ET processes in the array [91].

D'Souza and Da Ros have studied the effect of axial binding of pyridine on the photochemical stabilization of the complete CS states for a series of non-covalently and covalently linked porphyrin-fullerene dyads and supramolecular porphyrin-fullerene conjugates in different environments [13,24,69]. They have demonstrated that the axial coordination provides a strategy to control the charge separation and CR processes. The studies revealed that the charge separation reaction is slightly enhanced whereas the CR process becomes much slower by the pyridine coordination to the ZnP moiety because the ligand stabilizes the complete CS state [13,24,69].

Similarly to zinc porphyrin, zinc phthalocyanine (ZnPc) is an efficient emissive chromophore, and its singlet excited state has even longer lifetime than that of ZnP [92]. As the case for ZnP, the main effect of the axial coordination of ligands to ZnPc is the change in the energetic properties of this chromophore, but the influence of the ligand binding on the properties of ZnPc chromophore is not as strong as that observed on the ZnP chromophore. The differences in the energetic and spectroscopic features between the ligated and non-ligated ZnPc have been reported to be small [13]. For example, it has been demonstrated that absorption of ZnPc shifts to the blue by only 3 nm upon the axial coordination of imidazole-fullerene in a ZnPc-appended fullerene conjugate [13]. This impact difference arises from the differences in the electronic and redox properties between the ZnP and ZnPc chromophores [58]. The high electronic density distribution around the central zinc in the phthalocyanine macrocycle core may lower the

molecule's affinity to attract the ligand compared to the high affinity of the porphyrin chromophore.

3 Materials and methods

The primary goal of this research was to investigate the effect of the coordinating environment (such as electrolytes) on the exciplex intermediate and the whole reaction scheme of the ET taking place in the studied dyads. Therefore, the dyads were studied in the presence of negatively charged ligands, i.e. the chloride or bromide ions, in solvents of different polarities [I,II,IV] using a wide range of steady state and time-resolved spectroscopic techniques, and electrochemical methods [I,IV]. In addition, the reaction mechanism dependence on the solvent polarity was studied for porphyrin-fullerene dyads [III] in several solvents with different polarity.

3.1 Compounds

In this study, two different DA compounds were used: zinc porphyrin-fullerene dyads [I-III] and a zinc phthalocyanine-fullerene dyad [IV]. All the studied compounds were synthesized at the Department of Chemistry and Bioengineerig, Tampere University of Technology. The synthesis of the studied compounds is described in the literature [22,93], and the molecular structures are shown in Figure 3.1. All the studied DA dyads were double-bridged: the porphyrin or phthalocyanine donors are connected with the fullerene acceptor via two covalent linkers, which restricts the conformational freedom of the dyad. The zinc porphyrin and fullerene reference compounds, **ZnP-ref** and **C_{60}-ref** (Figure 3.1), were also studied. The chloride ion as a strong negatively charged ligand was produced from tetra-*n*-butylammonium chloride, TBACl [I,II,IV]. Tetra-*n*-butylammonium hexafluorophosphate, $TBAPF_6$, was used to create an ionic non-ligating environment as a reference [I].

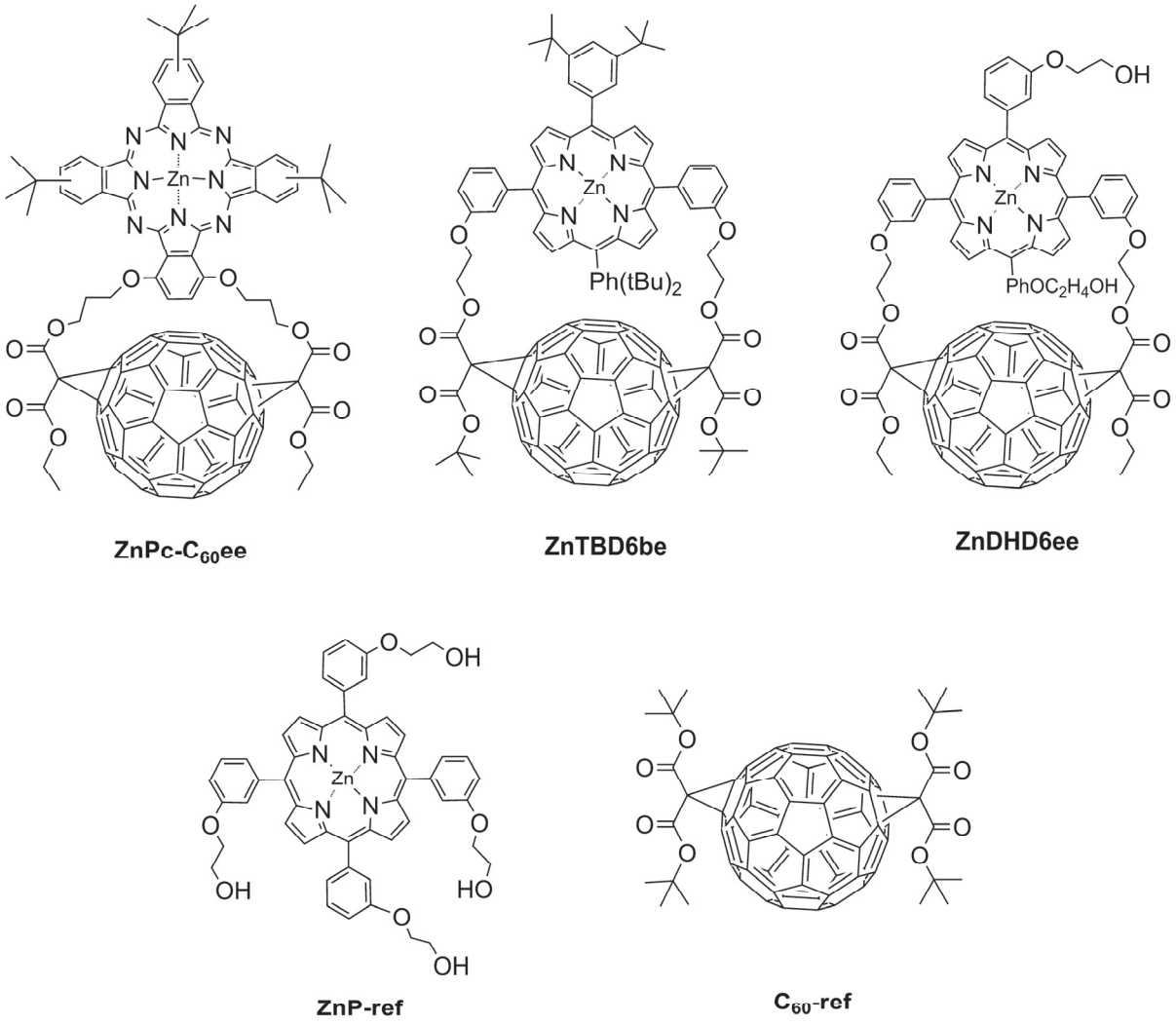

Figure 3.1. Molecular structures of the studied compounds: the two zinc porphyrin-fullerene dyads **ZnDHD6ee** and **ZnTBD6be** and their porphyrin and fullerene reference compounds, **ZnP-ref** and **C_{60}-ref**, and the zinc phthalocyanine-fullerene dyad **ZnPc-C_{60}ee**.

3.2 Steady state absorption and emission spectroscopy

The absorption spectra were measured using a Shimadzu UV-3600 spectrophotometer. The fluorescence spectra were recorded using a Fluorolog 3 fluorimeter (SPEX Inc.). The emission spectra were corrected using the correction function supplied with the instrument. Two different types of cuvettes were used in the absorption measurements, the glass and quartz cuvettes, depending on the measured spectral range. In the study of the CT absorption of **ZnDHD6ee** [II], the concentration of the dyad was set to give an absorption of about unity at the Q band of the dyad in 1 cm cuvette. Suitable excitation and monitoring filters were used in the fluorescence measurements.

3.3 Differential pulse voltammetry

The differential pulse voltammetry (DPV) was utilized to measure the oxidation and reduction potentials of the donor and acceptor species of the studied dyads, which are used to calculate the energies of the CS states of zinc porphyrin- and zinc phthalocyanine-fullerene dyads [I,IV]. The first one-electron oxidation potentials, E_{ox}, of the donors, ZnP and ZnPc, and the first one-electron reduction potential, E_{red}, of the acceptor fullerene in the dyad compounds were recorded with DPV in CH_2Cl_2 using a platinum wire as pseudo-reference electrode. A cell vial with 20 mL capacity was used as a three-electrode cell. A platinum disc working electrode (1 mm) was polished with alumina suspension and rinsed with ethanol and acetone before use. A graphite rod (0.5 mm) was used as a counter electrode.

The background signal was measured before running the DPV measurements of the dyads using $TBAPF_6$ and TBACl as supporting electrolytes for the non-ligating and chloride-ligating solutions, respectively. After measuring the background, 0.1 M of $TBAPF_6/CH_2Cl_2$ and $TBACl/CH_2Cl_2$ solutions of the samples were added to the electrochemical cell. The concentrations of the samples in the cell were 0.15-0.2 mM. Ferrocene was used as an internal reference redox system. Redox potential of Fc (~0.7 mM) was recorded in both salt solutions in separate measurements [I]. All the measurements were carried out at room temperature under high-purity nitrogen flow, and recorded using a potentiostat controlled by a computer. The scanning rate was 50 mV/s, the pulse time was 20 ms, the pulse amplitude was 20 mV, and the equilibration time was 5 s. All the measurements were done towards both the anodic and

cathodic directions and the oxidation and reduction potentials were obtained as an average of the two scans.

The DPV measurements of the reference compound (**ZnP-ref**) of the zinc porphyrin-fullerene dyad [I] were carried out also in $TBABF_4$/anisole electrolyte and using Ag/AgCl reference electrode to compare with the results obtained from the DPV measurements done versus the Pt wire pseudo-reference electrode. This three-electrode cell had a capacity of 3 mL, 1 mm platinum was used as the working electrode, Ag/AgCl as the pseudo-reference electrode, and a graphite rod (0.5 mm) as the counter electrode.

The energy of the complete CS state, ΔG_{cs}, in both the ligated and non-ligated dyads can be calculated using the Rehm-Weller equation, from the difference between E_{ox} and E_{red}, and accounting for the Coulombic attraction between the anion and cation as follows [30]:

$$\Delta G_{cs} = E_{ox} - E_{red} - \left[\frac{z_{D^+} z_{A^-} q_e^2}{4\pi\varepsilon_0 \varepsilon_r R_{DA}} \right], \tag{3.1}$$

where z_{D+} and z_{A-} are the charge numbers of the donor and acceptor species, respectively.

The Coulombic potential is calculated in point-to-point approximation and it increases the energy of the complete CS state [30]. Assuming that the binding does not change the geometry of the dyad, the Coulombic term is approximately the same for both ligating and non-ligating environments. The center-to-center distance for both of the studied zinc porphyrin-fullerene dyads [I,III] was previously estimated as 7 Å [12], which resulted in large values of the Coulombic term in non-polar and moderately polar solvents (e.g. 0.46 eV in anisole). For the zinc phthalocyanine-fullerene dyad [IV] R_{DA} was longer (13 Å) [22], which decreases the value of the Coulombic interaction between the phthalocyanine and fullerene moieties.

3.4 Time-resolved spectroscopy

Time-resolved spectroscopy is used to monitor the evolution of the photoinduced reactions, and determine the lifetimes of the transient states formed in different steps of the excitation relaxation process. In these measurements, the samples are excited by short laser pulses at an appropriate wavelength to generate an excited state. The excited state absorption spectrum is different from that of the ground state. Therefore, the time evolution of the transient states can be

monitored by measuring the absorbance or fluorescence of the sample as a function of time. In both absorption and emission measurements, the objective is to determine the impulse response function of the sample, i.e. the decay, which would be observed if the excitation pulse was infinitely short.

3.4.1 Pump-probe

The pump-probe method is used to measure the transient absorption spectra in the picosecond and subpicosecond time scales [94,95]. An optical scheme for pump-probe experiments is presented in Figure 3.2. The first key part of the laser system is a Ti:sapphire pulse generator pumped by Nd:YVO_4 laser (Verdi V6). The Ti:sapphire laser generates 50 fs pulses and it is tuned to operate at wavelength around 800 nm. The femtosecond pulses of the Ti:sapphire generator are amplified by a multipass amplifier pumped by a second harmonic of the Nd:YAG Q-switched laser. The amplified pulses are split into two beams. One beam is directed to a second harmonic generator (SHG) to produce the excitation (pump) pulses and the other part is focused to a water cuvette to generate white continuum pulse, which is used as the probe for monitoring the differential absorption of the samples. The probe beam is further split into two parts: a signal beam and a reference beam, which are both focused on the sample cuvette. The pump beam goes through a delay line with a moving right angle reflector. The delay line is used to tune the optical path length of the pump pulse relative to the probe pulse. The signal and reference beams cross the sample at different points and the pump pulse overlaps only with the signal beam. The pump pulse arrives at the sample before the probe pulse (the signal beam), and thus one can measure the absorption of the sample at a given delay time after the excitation. By moving the right angle reflector of the delay line one can change the delay between the pump and probe pulses and detect changes in the absorption in the time interval up to 1.2 ns. The upper delay limit is due to the limited length of the delay line. Typically 100-200 pulses were averaged at each delay time to improve the signal-to-noise ratio. The typical time resolution of the instrument is ~ 200 fs. The transient absorption spectra were recorded with a charge-coupled device (CCD) detector coupled with a monochromator in the visisble-near IR range.

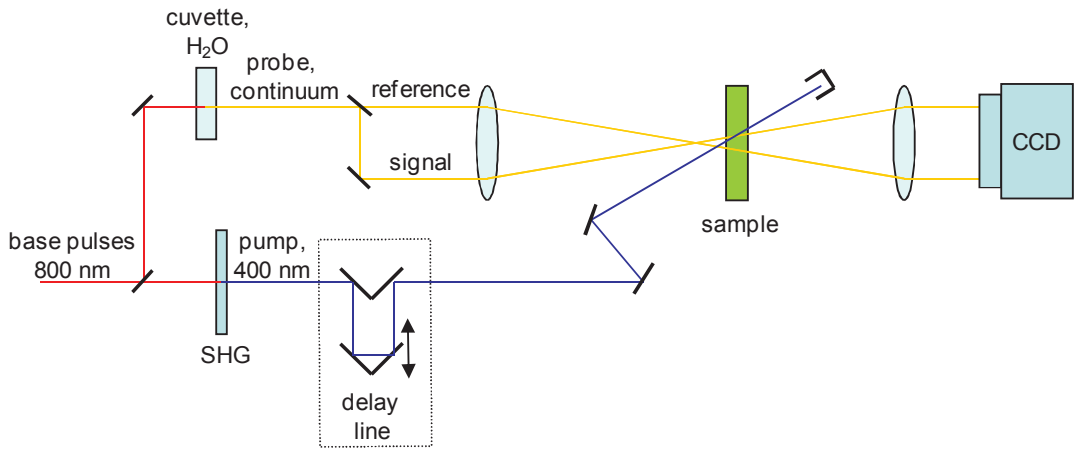

Figure 3.2. Scheme of the pump-probe technique [96]. SHG is a second harmonic generator and CCD is a charge-coupled device detector.

3.4.2 Up-conversion

The up-conversion technique for time-resolved fluorescence measurements in the picoseconds and subpicosecond time domains is used to detect the short-living emitting states [94,95]. An optical scheme of an instrument implementing the frequency up-conversion method is shown in Figure 3.3. The same femtosecond Ti:sapphire laser utilized in the pump-probe measurements was used in this method. To excite the sample in up-conversion measurements, a dichroic mirror is installed after the SHG to split the pulses into two beams. The reflected beam is used for the excitation while the transmitted one serves as the gate pulses. The collected sample emission by a lens is filtered to reject the excitation and then focused on to a non-linear crystal (NLC). The gate pulses pass through a delay line before the arriving at the NLC to mix with the sample emission. The NLC mixes the gate fundamental frequency, v_g, and the emission frequency, v_{em}, to produce the sum frequency or the signal frequency, $v_d = , v_g + v_{em}$. The intensity of the light at v_d is measured by the detection system (PD, Figure 3.3). The method is called up-conversion because the frequency of the signal is shifted up by the value v_g relative to the frequency of the emission v_{em}. The typical time resolution of the instrument is similar to that of the pump-probe method (~ 200 fs).

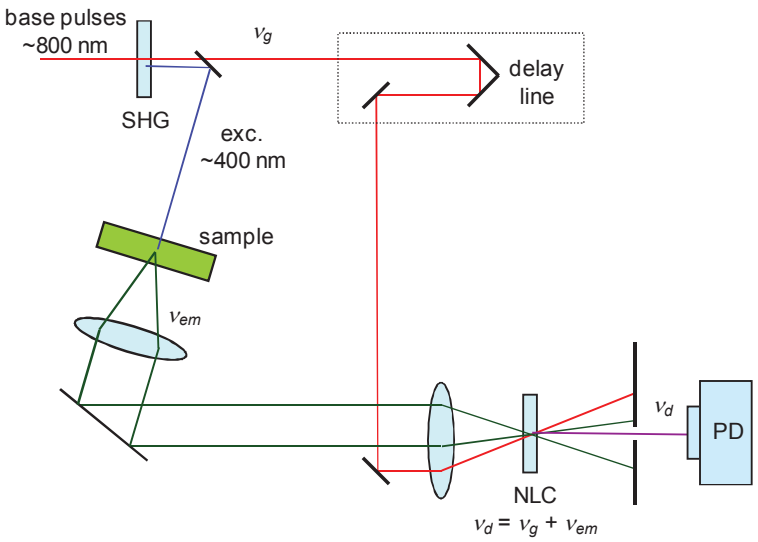

Figure 3.3. Scheme of the up-conversion time-resolved emission measurements [96]. NLC is a non-linear crystal and PD is a photodetector.

The up-conversion method was utilized to measure the emission decay profiles of **ZnDHD6ee** (Figure 3.1) using photo-excitation at ~ 405 nm, which promotes the zinc porphyrin moiety of the dyad to its second singlet excited sate. This state was not detectable in the measurements since the relaxation to the first singlet excited state via internal conversion is very fast. The fluorescence decay of **ZnDHD6ee** was monitored at the wavelength of maximum fluorescence intensity of each non-ligated and chloride-ligated zinc porphyrin chromophore (paper I).

3.4.3 Time-correlated single photon counting

The time-correlated single photon counting (TCSPC) system [95] (Figure 3.4) was mainly used to determine the lifetime of the exciplex state for the studied zinc porphyrin-fullerene dyads (Figure 3.1), by measuring the exciplex emission decay in the red-near IR region of the spectrum [I,III].

The pulsed light from a laser is used to excite the samples. The driver of the pulsed laser generates triggering pulses ("start" pulses) synchronized with the excitation light pulses. The sample emission is collected by a lens and passed to a photomultiplier tube (PMT) coupled with a monochromator. The photomultiplier works in photon counting mode, e.g. each detected photon generates an electric pulse on the photomultiplier output. The triggering electric pulse

and the pulse from PMT coming via the constant fraction discriminators (CFD) are directed to the time-to-amplitude convertor (TAC), which is the pulse controlled generator of linearly rising voltage. The pulse coming from CFD starts the generator operation (the "start" pulse). After the start pulse the TAC output voltage increases linearly with time. The emission photon pulse stops the generator and therefore it is called "stop" pulse. The output voltage of TAC is analyzed by the multichannel analyzer (MCA). The analyzer has a memory divided into a number of channels and each channel is associated with a voltage interval and thus each channel corresponds with a delay time interval (Figure 3.4).

The excitation wavelength used in the present study was 405 nm, and the time resolution of the TCSPC instrument was approximately 60-80 ps (FWHM of the instrument response function).

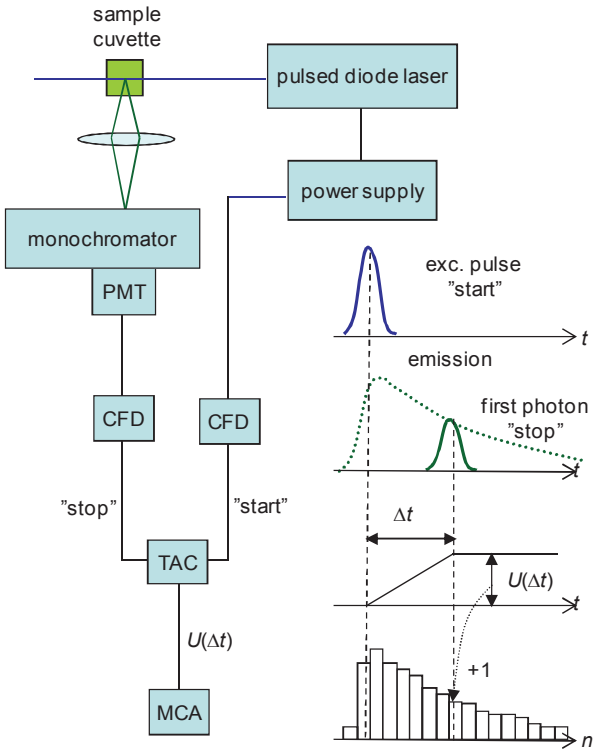

Figure 3.4. Scheme of the TCSPC measurement system [96]. PMT is a photomultiplier tube, CFD is a constant fraction discriminator, TAC is a time-to-amplitude convertor, and MCA is a multichannel analyzer.

3.4.4 Transient data analysis

The raw data obtained from the time-resolved measurements correspond to the populations of the transient states involved in the excitation-relaxation processes of the studied molecules. These data can be presented as a series of transient decay curves at different wavelengths. The data of the time-resolved measurements can be analyzed by fitting the decay curves to exponential functions, when all the reactions in the excitation relaxation process obey the first-order reactions as follows [95]:

$$F(\lambda,t) = \Sigma a_i(\lambda) \exp\left[-\frac{t}{\tau_i}\right], \tag{3.2}$$

where F is the model decay functions, e.g. it can be the differential absorption (ΔA) or the emission intensity (I) of the sample, λ is the wavelength, a_i are the pre-exponential factors or amplitudes, t is the time, and τ_i are the lifetimes of the components. The large data arrays obtained from time-resolved spectroscopic experiments can be analyzed by two strategies: the target analysis techniques or the global analysis [97]. For example, when there are two transient states absorbing at different wavelengths (Figure 3.5a) their absorption decay in time (the so-called kinetic traces, Figure 3.5b) can be monitored at specific wavelengths. In the target analysis one could simply take one wavelength specific for particular intermediate state and look at its evolution in time [97].

In the global data analysis a large amount of data at studied wavelengths is fitted simultaneously to obtain common lifetimes, τ_i, and component spectra, $a_i(\lambda)$, using the kinetic model given in Equation 3.2. This strategy is usually carried out when the spectral separation of two or more than two transient species is impossible or complicated. The transient absorption results can be presented as so-called decay component spectra, $a_i(\lambda)$, which are obtained from the fitting, and plotted as a function of wavelength (Figure 3.5d).

The number of components needed for the data fitting equals the number of transient species in the reaction, and in a simple case of a linear chain of reactions the rate constants of the reaction steps are inverse values of the fitted lifetimes. The quality of the fitting is indicated by the mean square deviation, σ^2, of the fitted parameters from the measured ones. The number of the exponential functions needed for the fitting was selected according to the enhancement in the fit

quality by adding exponential functions gradually. The limit of 10% decrease in σ^2 was considered as the tangible improvement in a fit procedure over another one, which has one exponent less than the other.

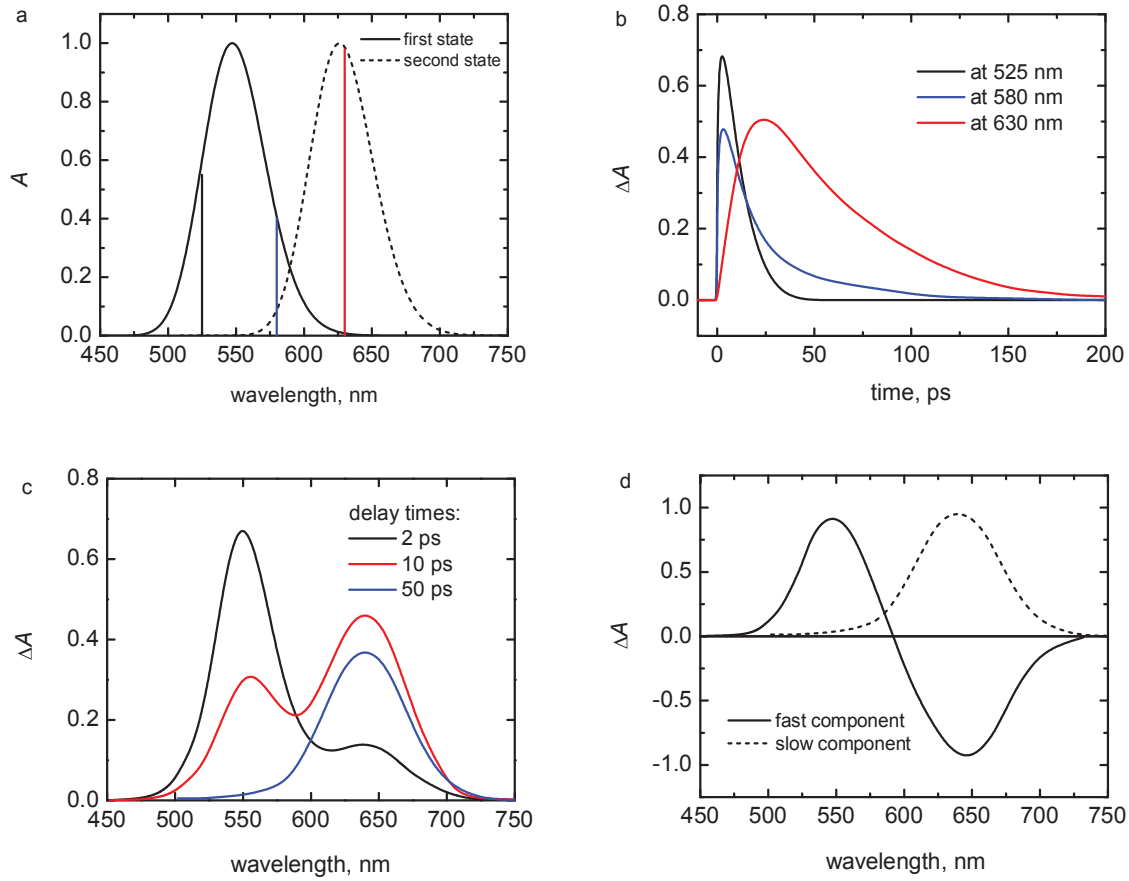

Figure 3.5. Transient data analysis procedure of two transient states resolved in the picosecond time domain and absorbing at different specific wavelengths: (a) absorption spectra of first instant state (solid) and delayed second state (dashed), the black, blue, and red lines indicate different detection conditions, (b) transient absorption decays (kinetic time traces) monitored at three different wavelengths, (c) transient absorption spectra at three different delay times, and (d) the pre-exponential factors obtained from the data fitting using Equation 3.2.

The emission decays of the transient states can be measured at different monitoring wavelengths with a constant accumulation time. As similar to the transient absorption data, the emission decay curves at different wavelengths can be fitted globally to obtain the emission decay associated spectra (DAS). With the aid of DAS, the different emitting species can be

distinguished and in some cases identified by comparing the shapes of the components to the steady state fluorescence spectra. In this study, DAS were measured with TCSPC to resolve the emitting exciplex state which overlaps with the emission of the first singlet excited states of the zinc porphyrin-fullerene dyads [I,III].

4 Results and discussion

4.1 Theoretical model for quantitative analysis of ET in donor-acceptor dyads

In earlier studies an exciplex has been clearly identified as a transient state in the photoinduced reactions of the zinc porphyrin-fullerene dyads used in this study (Figure 3.1) in both polar and non-polar media [12]. The CT absorption and emission bands in the red to near IR spectrum range have been clearly observed [12,31]. It has been found that the complete CS state does not form in non-polar solvents but the exciplex produced from the singlet excited state of porphyrin relaxes directly to the ground state. In polar solvents, the exciplex has been observed as an intermediate between the locally excited state of porphyrin and the complete CS state [12].

When the photo-reaction in a porphyrin-fullerene dyad is initiated by exciting the porphyrin chromophore, the clear distinction between the exciplex and the complete CS state in the dyads is a challenging task because of two reasons: 1) the ET reaction does not proceed in one step and a few intermediate states have to be identified and distinguished, and 2) the differential spectrum of the exciplex has features resembling the differential spectra of both the porphyrin singlet excited state and the complete CS state. If the locally excited state of porphyrin is not formed, the number of intermediate states involved in the excitation-relaxation process of the dyad will be decreased to only two intermediates [see paper III]. This strategy can be performed by exciting the dyad in the near IR region, which populates the exciplex directly from the ground state.

Generally, if a DA system has strong interaction between the donor and the acceptor, the exciplex state can be formed and it may have sufficiently long lifetime to undergo light emission [34-36]. Such DA pairs are characterized by relatively strong oscillator strength for the transition from the ground state to the exciplex (the CT band) and the quantitative analysis of the ET reaction can be simplified. Upon the photo-excitation of the dyad at the CT band, a direct population of the exciplex from the ground state occurs. The exciplex can relax to the ground state or form the complete CS state, which in turn recombines to the ground state (Scheme 4.1).

The populations of both the exciplex and the complete CS state are indicated by their transient absorption spectra. The pump-probe method can be used to measure the absorption of the transient states in the picoseconds to sub-picosecond time scales (Section 3.4.1). Such kind of

measurements supplies information that can be used to detect the exciplex and the complete CS state and in turn to identify the whole ET reaction mechanism of the dyad in different environments. The absorption decays of the exciplex and the complete CS state can be resolved into two exponential components.

Since the exciplex is an emissive state, direct decay of this state to the ground state can also be monitored by measuring the emission decays in non-polar and moderately polar solvents [12,17,41,46,47,49,50]. The time-resolved emission measurements give information on the concentration of the exciplex only, but not on that of the complete CS state. If a significant back reaction from the complete CS state to the exciplex takes place, the exciplex emission decay will be bi-exponential with the same time constants as the absorption decay [98,99]. In fact, the occurrence of conversion from the complete CS state to the exciplex can be observed as a bi-exponential kinetic behavior for the exciplex in an emission experiment. The quality of the TCSPC experiments (Section 3.4.3) is usually very high, allowing the bi-exponential analysis to be performed.

The photo-excitation of the dyad at the CT band in the time-resolved absorption measurements results only in two intermediate states: the exciplex generated directly after the excitation, and the complete CS state. Therefore, only three states are involved in the excitation-relaxation scheme: the ground state, DA, the exciplex, $(DA)^*$, and the complete CS state, $D^{\bullet+}A^{\bullet-}$, (Scheme 4.1). It has been earlier shown [12,41] that depending on the solvent polarity the energy of the complete CS state can be either lower (in polar media) or higher (in non-polar media) than that of the exciplex. Generally, an equilibrium between the exciplex and the complete CS state can be expected (Scheme 4.1). Relaxation of $(DA)^*$ and $D^{\bullet+}A^{\bullet-}$ to the ground state are described by four rate constants depicted in Scheme 4.1: the direct relaxation of the exciplex to the ground state, k_{ex}, the transition from the exciplex to the complete CS state, k_{ET}, the back reaction from the complete CS state to the exciplex, k_{cx}, and the decay of the complete CS state to the ground state or the CR process, k_{CR}.

Scheme 4.1. Reaction scheme of the excitation-relaxation process of **ZnTBD6be**.[a]

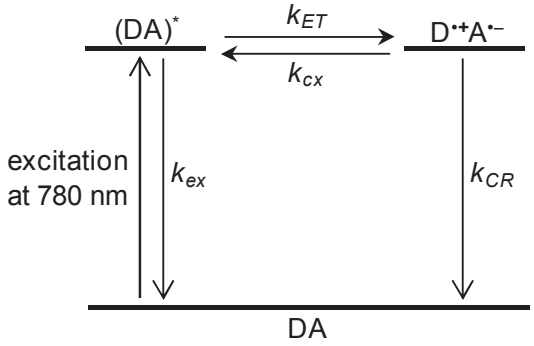

[a] k_{ET} and k_{CR} are the rate constants for the charge separation and charge recombination processes, respectively, k_{cx} is the rate constant for the back conversion of the complete CS state to the exciplex, and k_{ex} is the relaxation rate constant of the exciplex to the ground state.

There are only two transient states associated with Scheme 4.1, and the apparent lifetimes of the states depend on four intrinsic rate constants, in a general case. Therefore, not much information about the intrinsic reaction rate constants can be obtained by using solely the experimental lifetimes. The essential information can be obtained from the transient absorption component spectra and emission DAS (Section 3.4.3). In polar solvents the energy of $D^{\bullet+}A^{\bullet-}$ is considerably lower than that of $(DA)^*$ and the equilibrium between these two states is shifted more to the side of $D^{\bullet+}A^{\bullet-}$, i.e. $k_{ET} >> k_{cx}$ and the reaction $D^{\bullet+}A^{\bullet-} \rightarrow (DA)^*$ can be neglected. On the contrary, in non-polar media the energy of $D^{\bullet+}A^{\bullet-}$ is higher than that of $(DA)^*$, $k_{ET} << k_{cx}$, and the reaction $(DA)^* \rightarrow D^{\bullet+}A^{\bullet-}$ can be neglected. Apparently, in an intermediate case neither of these reactions can be neglected, and a more advanced analysis method has to be developed to obtain information on the reaction parameters. The following discussion describes the relations between the intrinsic rate constants and the ET parameters, the construction of the model that accounts for all four reactions depicted in Scheme 4.1, and the strategy used to find a connection between the intrinsic rate constants and the two observable lifetimes.

The kinetics of the relaxation process of the DA dyad (Scheme 4.1) can be considered from the thermodynamic point of view. For an established equilibrium, the population ratio between the exciplex and the complete CS state does not change in time and is given by the Boltzmann distribution:

$$\frac{[ex]}{[cs]} = \exp\left[-\frac{(\Delta G_{ex} - \Delta G_{cs})}{k_B T} \right], \tag{4.1}$$

where $[ex]$ and $[cs]$ are the populations, ΔG_{ex} and ΔG_{cs} are the free energies of the exciplex and the complete CS state, respectively, k_B is Boltzmann's constant, and T is the temperature.

Right after the excitation at the CT absorption band, only the exciplex is populated and the thermodynamic equilibrium between the exciplex and complete CS state is established with the rate constants k_{ET} and k_{cx} according to Scheme 4.1. This is observed as the fast component in the time-resolved absorption measurements, i.e. the fast process represents the transition reaction between the exciplex and the complete CS state. The relaxations are considered under the condition of established thermodynamic equilibrium (Equation 4.1), which formally means that $k_{ET} + k_{cx} > k_{ex}$ and k_{CR}, and the exciplex and complete CS state relax synchronously, even though the relative populations of the states may be very different in different solvents.

According to this assumption, the common relaxation rate constant depends on the relative ratio between the populations of the states as follows:

$$k_{fit} = k_{ex}\beta_{ex} + k_{CR}\beta_{cs} = k_{ex}\beta_{ex} + k_{CR}(1 - \beta_{ex}), \tag{4.2}$$

where k_{fit} is the common decay rate constant (see Section 4.2), and β_{ex} and β_{cs} are the relative fractions of the exciplex and the complete CS state, i.e. $\beta_{ex} = [ex]/([ex]+[cs]) = ([ex]/[cs])/([ex]/[cs] + 1)$ and $\beta_{cs} = [cs]/([ex]+[cs])$.

The direct relaxation rates of the exciplex and the complete CS state to the ground state (either k_{ex} or k_{CR} in Scheme 1) can be obtained from Equation 2.7 (Section 2.1) [25-27,29]. The vibrational energy and the electronic-vibrational coupling have similar values for the exciplex and the complete CS state relaxation, but the electronic coupling, the free energy, and the reorganization energy are clearly different for these two reactions.

The dependences of the reorganization and free energies on the solvent polarity factor [26,28,30,31] were discussed in Sections 2.1 and 2.2, respectively. The dependence in Equation 2.6 (Section 2.2) deals with complete charge separation, but in the case of an exciplex a partial charge separation is expected and the elementary charge q_e in the equation should be replaced by

the amount of charge being separated, which is equal to the multiplication of q_e by the charge separation degree (γ) in the exciplex as follows:

$$b = \frac{q_e^2 \gamma^2}{4\pi\varepsilon_0}\left[\frac{1}{2R_D} + \frac{1}{2R_A} - \frac{1}{R_{DA}}\right], \tag{4.3}$$

The charge separation degree is unity in the case of the complete CS state and $0 < \gamma < 1$ for the exciplex state.

Similar square dependence of the free energy coefficient (a) on the charge separation degree (γ) in the exciplex can still be expected in case of the complete CS state. In this case the coefficient a can be calculated from the corresponding coefficient of the exciplex and its charge separation degree, without knowing the center-to-center distance between the donor and acceptor (R_{DA}, Equation 4.3), which may differ from the geometrical distance between the donor and the acceptor:

$$a_{cs} = a_{ex} / \gamma^2, \tag{4.4}$$

where a_{ex} and a_{cs} are the free energy coefficients of the exciplex and the complete CS state, respectively, and γ is the charge separation degree in the exciplex.

The dependence of the total reorganization energy (λ_r) of the exciplex on the solvent polarity factor (f_s) has been found to be linear as presented in Equation 2.5 (Section 2.1) [31]. The inner sphere or the internal reorganization energy does not depend on the solvent polarity [26]. Similarly to the free energy case, the solvent dependent part of the reorganization energy (the coefficient b in Equation 2.5) of the complete CS state can also be calculated from the corresponding value of the exciplex and the charge separation degree as follows:

$$b_{cs} = b_{ex} / \gamma^2, \tag{4.5}$$

where b_{ex} and b_{cs} are the reorganization energy coefficients for the exciplex and the complete CS state, respectively. Therefore the solvent dependences of the free and reorganization energies of both the exciplex and the complete CS state can be modeled by guessing γ, E_0, and λ_{ri} values for the two states and using the a_{ex} and b_{ex} coefficients estimated previously [31].

Knowing the populations of the exciplex and the complete CS state (Equation 4.1), and their free energies (Equation 2.9), one can calculate the rate constants of the equilibrium reaction between them, k_{ET} and k_{cx}, in all of the studied solvents. In equilibrium $k_{ET}/k_{cx} = [cs]/[ex]$ and $\tau_{fast} = (k_{ET} + k_{cx})^{-1}$, which leads to

$$k_{ET} = \left[\frac{1-\beta_{ex}}{\tau_{fast}} \right], \tag{4.6}$$

where τ_{fast} is the experimental lifetime of the fast component obtained from the data analysis of the time-resolved absorption spectroscopy.

Substituting Equations 2.5, 2.7, 2.9, 4.1, 4.4, and 4.5 into Equation 4.2, a mathematical model to calculate the common lifetimes ($1/k_{fit}$) and to fit the dependence of the lifetimes on the solvent polarity can be constructed. The model was successfully applied to analyze the solvent dependence of a porphyrin-fullerene DA dyad having a close contact between the porphyrin donor and the fullerene acceptor (**ZnTBD6be**, Figure 3.1) and it can be valid for any DA system having high enough electronic coupling for the exciplex-ground state transition. Previously reported exciplex parameters for **ZnTBD6be** [31] were used as fixed parameters during the fit process [see paper III].

4.2 Model application to a porphyrin-fullerene dyad

The theoretical model derived in Section 4.2 was developed to analyze the ET processes occurring in the porphyrin-fullerene dyads, which have a face-to-face orientation between the porphyrin donor and fullerene acceptor (Figure 3.1). A clear quantitative distinction between the exciplex and the complete CS state was obtained by applying the constructed model to a porphyrin-fullerene dyad in all of the studied environments even though the transient absorption spectra of these two states were rather similar.

The excitation wavelength of the dyad was set at 780 nm (at the CT band) in the pump-probe measurements, which populates the exciplex directly from the ground state. A wide range of solvents with different polarities (from non-polar toluene to strongly polar DMF) was used in these measurements. The pump-probe measurements confirmed the ET reaction reported earlier for **ZnTBD6be** [12] and revealed similar shapes of the transient absorption decay component

spectra of the dyad in all of the studied solvents (see spectra in DMF as an example in Figure 4.1). The time constants of the resolved components were very different in different environments. The time constants of both the fast and the slow components decrease with the increase of solvent polarity (Table 4.1) following the trend previously reported for similar dyads **[12,41,46,47]**. In all solvents, except in toluene, two components were resolved from the fitting of the transient absorption spectra (paper III).

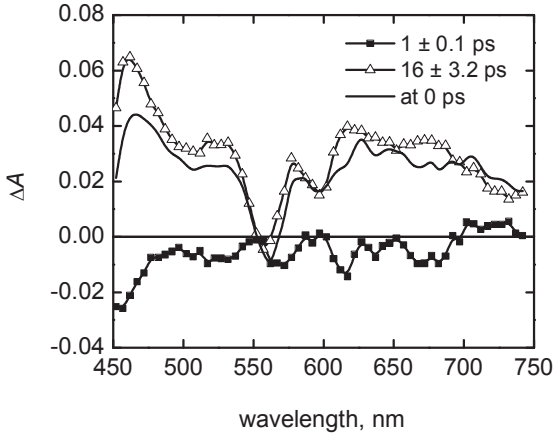

Figure 4.1. Transient absorption decay component spectra (solid lines with symbols) and time resolved transient absorption spectrum right after excitation (at 0 ps, dashed line) for **ZnTBD6be** in DMF. The excitation wavelength was 780 nm.

The relaxation of the exciplex was monitored by measuring its emission decay in the near IR region of the spectrum using the TCSPC method [12,41,46,49]. The instrument time resolution was not sufficient for determining the emission lifetimes in solvents with polarities higher than that of anisole (i.e. for solvents with $\varepsilon_r > 4.3$), where the exciplex emission has a too short lifetime and minor population. The decays were measured in the wavelength range of 580-840 nm, fitted globally, and the DAS (see Section 3.4.3) were used to assign the correct lifetime to the exciplex decay [41,49]. The mechanism of the excitation-relaxation process of the dyad obeys Scheme 4.1 (Section 4.1) and the experimental lifetimes of **ZnTBD6be** measured with TCSPC in toluene, anisole, and toluene/anisole are presented in Table 4.1.

Table 4.1. Experimental lifetimes of **ZnTBD6be** obtained from the TCSPC and pump-probe measurements in different solvents.

solvent	τ (ps)[a]	τ_{fast} (ps)[b]	τ_{slow} (ps)[b]
toluene	1260	-	1120
toluene/anisole	325	12.6	331
anisole	142	9.8	177
DCB	-	8.7	154
anisole/PhCN	-	4.2	62
PhCN	-	2.5	46
DMF	-	1.0	16

[a] From TCSPC. [b] From pump-probe.

A set of energetic fit parameters for the exciplex and the complete CS state was obtained from the quantitative analysis (Table 4.2). The dependence of the calculated common lifetimes ($1/k_{fit}$) on the solvent polarity factor is shown in Figure 4.2.

Table 4.2. Energetic parameters obtained from the fit. E_0 is the solvent independent part of the free energy, γ is the charge separation degree, λ_{ri} is the internal reorganization energy, and V is the electronic coupling matrix element.

state	E_0 (eV)	λ_{ri} (eV)	γ	V (eV)
exciplex	1.199	0.082 [a]	0.55	0.254
complete CS	1.072	0.105	1 [b]	0.012

[a] From ref. 31. [b] Fixed value.

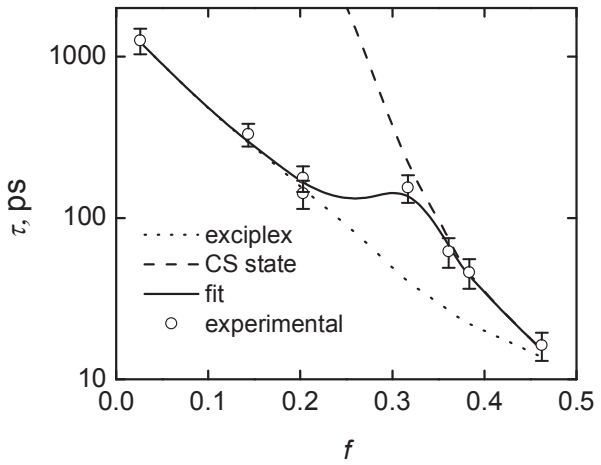

Figure 4.2. Dependence of the measured decay time constants (long-lived component, Table 4.1) of **ZnTBD6be** on the solvent polarity factor (circles with error bars), fitted dependence of the common calculated lifetimes (solid line), and separate time constants for the direct relaxation of the exciplex and the complete CS state to the ground state (dotted and dashed lines, respectively).

The detailed discussion on the fit parameters given in Table 4.2 and the comparison between the obtained parameters for the exciplex with the corresponding ones reported previously is presented in paper III. It was concluded that the electronic couplings, the solvent independent parts of the free energies of both the exciplex and the complete CS state, and the charge separation degree in the exciplex were determined accurately and they can be considered more reliable than the ones reported earlier, assuming that the applied model is valid. A special attention was paid to the electronic couplings for both the exciplex and the complete CS state. The obtained electronic coupling for the exciplex of **ZnTBD6be** was approximately 4 times larger than those reported earlier for such dyads [12,17,47]. This difference can be explained by the different strategy used to calculate the electronic coupling. In all previous studies the value of the electronic coupling was calculated from the estimation of the oscillator strength of the CT absorption band and the center-to-center distance between the donor and the acceptor (Equation 2.12), which are prone to be evaluated with rather large inaccuracy. In this study the electronic coupling was not obtained from a single measurement in one solvent but achieved from applying a theoretical model, which was found to be valid in a wide range of environments, and was used

successfully for quantitative analysis of the photodynamic reactions of the dyad (Scheme 4.1) in both polar and non-polar solvents.

The mathematical model derived in Section 4.2 can be used to obtain the ET parameters for such systems at any value of solvent polarity. The calculated rate constants, k_{fit}, k_{cx}, k_{ET}, the measured rate constant of the slower component, k_{exp}, the relative populations of the exciplex, β_{cs}, and the free energies of both the exciplex and the complete CS state are given in Table 4.3.

Table 4.3. Calculated relative populations of the exciplex (β_{ex}), calculated free energies for the exciplex and the complete CS state (ΔG_{ex} and ΔG_{cs}, respectively), calculated rate constants obtained from the fit model, k_{ET}, k_{cx}, and k_{fit}, and the experimental direct relaxation rate constants of the exciplex and the complete CS state, k_{exp}, for **ZnTBD6be** in variable solvents.

solvent	ε_r	β_{ex} [b]	ΔG_{ex} (eV) [c]	ΔG_{cs} (eV) [c]	k_{ET} (s^{-1}) [d]	k_{cx} (s^{-1}) [e]	k_{fit} (s^{-1}) [f]	k_{exp} (s^{-1}) [g]
toluene	2.38	0.999	-1.346	-1.558	-	-	0.8×10^9	0.8×10^9 [h]
toluene/anisole	3.37 [a]	0.987	-1.303	-1.415	1.0×10^9	9.3×10^{10}	3.4×10^9	3.0×10^9 3.0×10^9 [h]
anisole	4.33	0.908	-1.279	-1.339	9.4×10^9	7.8×10^{10}	5.9×10^9	5.6×10^9 7.0×10^9 [h]
DCB	10.12	0.139	-1.234	-1.186	9.9×10^{10}	1.6×10^{10}	7.4×10^9	6.5×10^9
anisole/PhCN	14.88 [a]	0.057	-1.223	-1.149	2.2×10^{11}	1.4×10^{10}	1.4×10^{10}	1.6×10^{10}
PhCN	25.90	0.024	-1.213	-1.117	3.9×10^{11}	9.8×10^9	2.5×10^{10}	2.2×10^{10}
DMF	38.25	0.017	-1.208	-1.102	9.8×10^{11}	-	6.6×10^{10}	6.3×10^{10}

[a] The ratio of solvents was 1:1 (see paper III). [b] Calculated from Equation 4.1. [c] Calculated from Equation 2.9. [d] Calculated from Equation 4.6. [e] Derived from Equation 4.6. [f] Calculated from Equation 4.2. [g] From pump-probe (the slow component). [h] From TCSPC.

The results presented in Table 4.3, and the information about the relations between the experimental and the calculated intrinsic rate constants in the excitation-relaxation process of **ZnTBD6be** are discussed in paper III.

4.3 Effect of halide binding on ET in porphyrin- and phthalocyanine-fullerene dyads

In this Section, the investigations of the halide coordination effects on ET properties of zinc porphyrin- and zinc phthalocyanine-fullerene dyads (**ZnDHD6ee** and **ZnPc-C_{60}ee**, Figure 3.1) are discussed. The effect of chloride binding with the ZnP and ZnPc moieties on the photoinduced ET reaction of the dyads was investigated in solvents of different polarities ranging from moderately polar anisole to strongly polar DMF taking into account the solubility of the used electrolyte (TBACl salt) in the solvents. The free energies and the lifetimes of all the intermediates involved in the ET reactions (the singlet excited state, the exciplex, and the complete CS state) were affected by the ligation, but the strength of the effect ranged from considerable on the ET properties of the zinc porphyrin-fullerene dyad to weak on those of the zinc phthalocyanine-fullerene dyad.

4.3.1 Anion ligand effect on the singlet excited state of the donor

4.3.1.1 Zinc porphyrin-fullerene dyad

The absorption spectra of **ZnDHD6ee** (Figure 4.3a) in presence of chloride and bromide ions show clear red shift of all absorption bands and an increase in the intensity ratio of the high to low energy Q bands relative to that of the non-ligated dyad [87,89]. The Soret band of **ZnDHD6ee** in TBACl/anisole was shifted to the red by ~13 nm compared to the sample in anisole, while the Q bands were shifted to the red by ~20 nm, and the intensity of the Q_1 band increased by almost two times. Compared to the effect of the chloride, the red shift and the change in the intensity ratio were slightly larger with the bromide ion. It has been reported earlier that the red shift and changes in intensity upon the axial coordination of ligands to the zinc porphyrin is due to the charge and medium polarization induced by the halide ion, which leads a shift of electron density from the ligand toward the porphyrin ring via the central zinc [90].

The emission spectra of the non-coordinated and chloride-coordinated **ZnDHD6ee** are shown in Figure 4.3b. The non-ligated dyad showed a broad emission band above 770 nm, which was not observed for the chloride-ligated dyad. At the same time, the strong emission of the first singlet excited state (S_1) of zinc porphyrin chromophore was found to be efficiently quenched in both coordinated and non-coordinated cases [see paper I]. Such efficient quenching has been earlier

attributed to the fast formation of the intramolecular exciplex for **ZnDHD6ee** and similar double-linked zinc porphyrin-fullerene dyads [12].

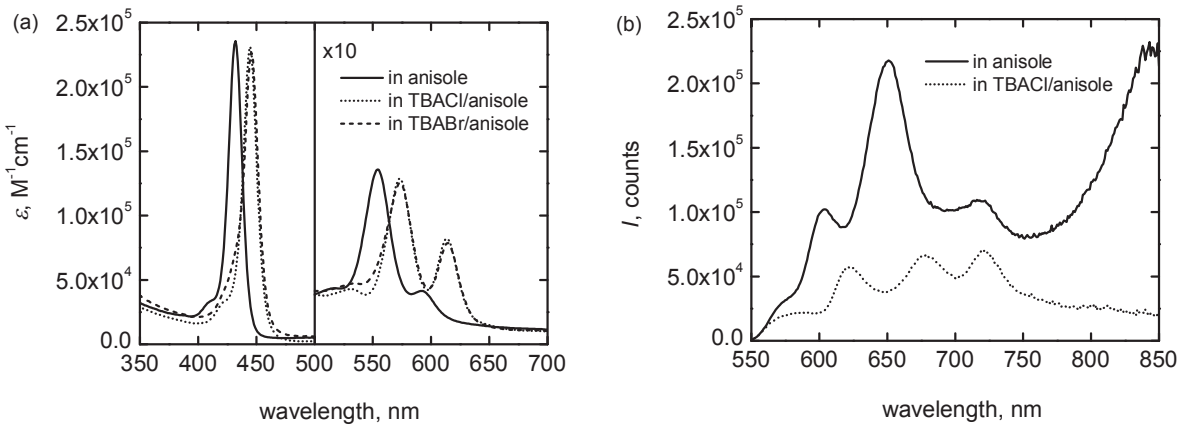

Figure 4.3. Steady state absorption and fluorescence spectra of **ZnDHD6ee** in anisole and in halide solutions: (a) absorption and (b) fluorescence. The Q band region in the absorption spectrum is magnified ten times for clarity.

The lifetime of the S_1 state of the ZnP chromophore in **ZnDHD6ee** was determined from time-resolved fluorescence measurements. The emission decay profiles of the dyad in the femto to picosecond time scales were measured with the up-conversion method (Section 3.4.2). The emission decays of the non-ligated and chloride-ligated dyads were monitored at the maximum fluorescence of the ZnP S_1 state (see paper I). In anisole, the lifetime of the S_1 state (0.5 ps) was slightly shortened upon the chloride coordination (0.4 ps in TBACl/anisole). The lifetime of the S_1 state of ZnP can also be measured with time-resolved absorption spectroscopy, i.e. pump-probe, but the up-conversion is more accurate method. As was explained above, in porphyrin-fullerene dyads the energies of S_1 state of porphyrin chromophore, the exciplex state, and the complete CS state are relatively close to each other and it is difficult to discriminate between their transient absorption spectra. Instead, in the up-conversion technique the emission decay of the S_1 state is monitored at a specific wavelength and its lifetime can be determined.

4.3.1.2 Zinc phthalocyanine-fullerene dyad

The absorption spectrum of **ZnPc-C_{60}ee** in the presence of chloride ions showed slight changes compared to that recorded in the corresponding non-ligating environment (Figure 4.4a). The entire absorption spectrum was blue shifted upon the axial binding and the absorption intensity ratio was changed. The Soret band of **ZnPc-C_{60}ee** in the coordinating solution was shifted to the blue by 5-7 nm compared to the corresponding spectra measured in pristine solvents, while the Q_1 band was shifted to the blue by 5 nm. In addition, the hyperchromic effect was observed for the Q_1 band, i.e. the intensity ratio between the Soret and Q_1 band (Soret/Q_1, see paper IV) in the coordinated dyad was decreased by 18-25 % relative to that of the non-ligated one. The blue shift phenomenon represents an opposite trend compared to that observed for the zinc porphyrin-fullerene dyad ligated with chloride.

Similarly to the absorption, the emission of the chloride-coordinated **ZnPc-C_{60}ee** was shifted to the blue by 5 nm, and a slight increase in the emission intensity of the Q_1 band upon the ligand binding was also seen. The emission spectra of **ZnPc-C_{60}ee** in DMF and TBACl/DMF are shown in Figure 4.4b.

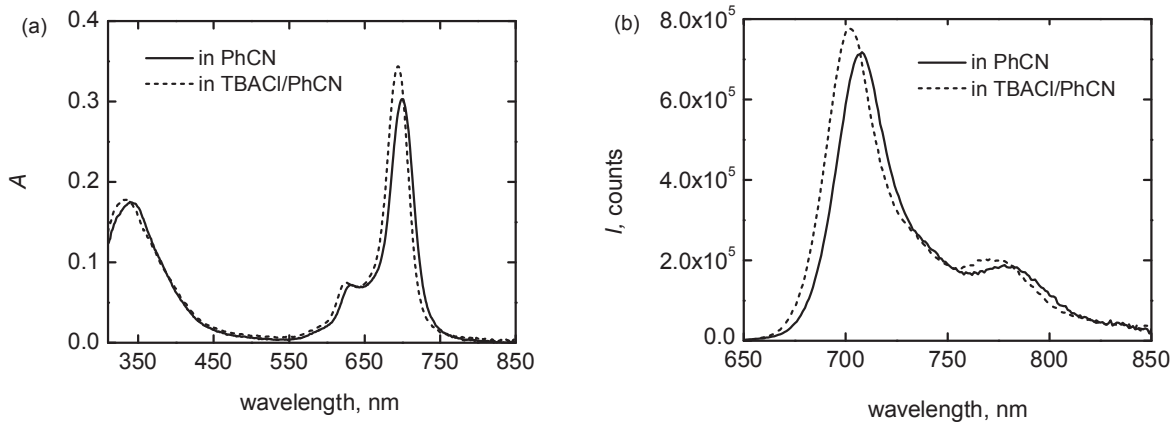

Figure 4.4. Steady state absorption and fluorescence spectra of **ZnPc-C_{60}ee** in non-ligating and chloride-ligating solutions: (a) absorption and (b) fluorescence.

The transition from the S_1 state of phthalocyanine to the complete CS state has been earlier proved for the free-base compound of **ZnPc-C_{60}ee** [22], and for other double-linked free-base and zinc phthalocyanine-fullerene dyads having the same linkers as of **ZnPc-C_{60}ee** [23]. An

efficient quenching of the ZnPc fluorescence by fullerene has been observed in both polar and non-polar media.

As shown in Figure 4.4b, no emission band characteristic for that of an exciplex was seen in either non-coordinated or chloride-coordinated dyads. The lifetime of the S_1 state of ZnPc was determined from the pump-probe measurements, and was found to be increased upon the coordination of chloride to the central zinc of the ZnPc chromophore. In all of the chloride-ligating solutions the lifetime of the S_1 state of ZnPc was 1.2-1.4 times longer than that in the corresponding non-ligating environment (see Section 4.4).

There were two important differences between the ZnP and ZnPc chromophores in the effect of chloride ligation on the free energies and lifetimes of the S_1 states. Firstly, the whole effect was weaker in the case of the zinc phthalocyanine-fullerene dyad, and secondly the trend was opposite: the chloride binding to the central zinc results in lower energy and shorter lifetime for the S_1 state of ZnP whereas it leads to an increase in both the energy and lifetime of the singlet excited state of ZnPc chromophore (Section 4.4).

4.3.2 Anion ligand effect on the intramolecular exciplex

The CT absorption band, which corresponds to the direct transition from the ground state to the exciplex was observed for the double-linked porphyrin-fullerene dyad in chloride and bromide salt solutions (Figure 4.5). Compared to the dyad in pristine environment, the CT absorption band is higher and broader, and shifted to the red gradually in the ligating environments. The red shift in the ligating solutions of the moderately polar solvents (anisole and THF) was found to be much larger than that in pure solvents with higher polarities. The halide coordination to the zinc porphyrin donor has a stronger effect on the exciplex features than a simple increase in medium polarity. This can be rationalized by the fact that the negative charge of the halide induces an electric field around the dyad near the porphyrin ring. The direction of the induced electric field is the same as the direction of ET, i.e. from porphyrin to fullerene, which makes the ET reaction a more efficient process. The effect of the electric field is expected to be strong on the CT absorption since in this state the static dipole moment of the molecule is much larger than that in the ground state. This was observed both as a gradual red shift of the CT absorption band and as a moderate increase in its intensity (Figure 4.5).

The CT emission band was clearly seen in moderately polar solvents (Figure 4.3b). The emission spectrum of **ZnDHD6ee** in anisole showed clear features of the exciplex above 770 nm in addition to ZnP fluorescence around 570-700 nm. The chloride binding resulted in an increase in the oscillator strength and large red shift of the CT absorption band (Figure 4.5), but the CT emission band was not detected (Figure 4.3b). This result indicates that the exciplex is efficiently quenched (its lifetime is shortened) upon the coordination of chloride ion to the ZnP moiety of the dyad.

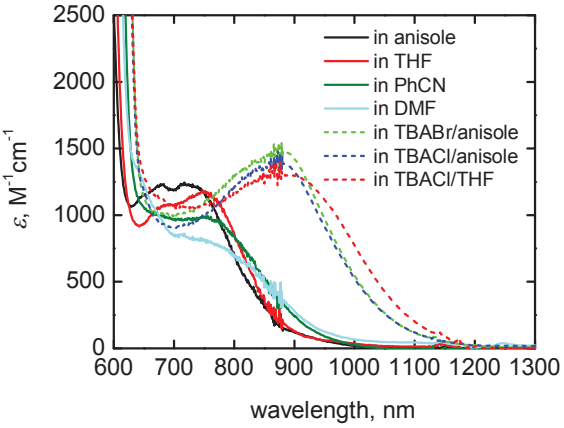

Figure 4.5. Absorption spectra of **ZnDHD6ee** and its complexes at the red and near IR regions of the spectrum in anisole, THF, PhCN, DMF, 0.3 M TBABr/anisole, 0.1 M TBACl/anisole, and 0.1 M TBACl/THF. The noisy signal around 870-885 nm is due to the change of the spectrophotometer detector.

The exciplex absorption and emission spectra can be analyzed using the semi-quantum Marcus theory for electron transfer [31,39,52]. The shape of the CT absorption band is given by Equation 2.11 (see Section 2.2 for the details). In fact, Equations 2.7, 2.10, and 2.11 (Sections 2.1 and 2.2) are derived in frame of one and the same ET theory and can be used for common analysis of the phenomenon. Since the CT emission was not observed in the halide ligated dyads (Figure 4.3b), only the CT absorption spectra were used in this analysis. Because the CT absorption band overlaps partially with the lowest energy absorption bands of the fullerene and porphyrin chromophores, Equation 2.11 cannot be used directly to fit the spectra presented in Figure 4.5. Instead, the fitting of the absorption spectra of the dyad was done after subtraction of the absorption of the fullerene reference compound, **C_{60}-ref** (Figure 3.1), from that of the dyad (see paper II for a more detailed discussion), and taking into account the ZnP absorption bands. The

fit model included a total of three bands (Figure 4.6): the CT absorption band as given in Equation 2.11, a sharp Gaussian for the first Q band of zinc porphyrin, and a broad Gaussian band with a maximum outside of the fit range in the blue part of the spectrum, which accounts for all other absorption bands.

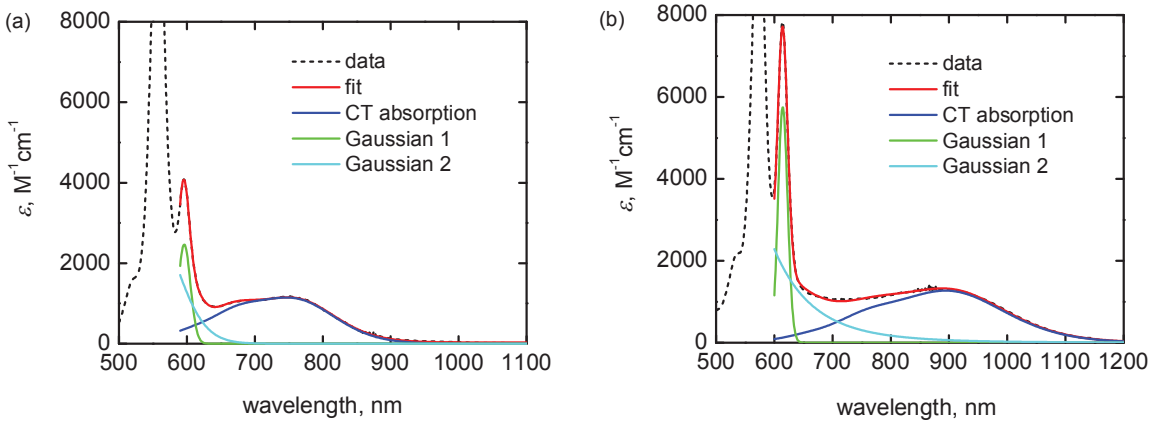

Figure 4.6. Fitted (solid red lines) and measured (dashed lines) absorption spectra of **ZnDHD6ee**: (a) in THF and (b) in 0.1 M TBACl/THF. The components of the absorption fit function are the CT band (blue line), and two Gaussian bands (light blue and green lines).

The energetic parameters obtained from the fitting of the CT absorption band in the studied ligating and non-ligating environments are presented in Table 4.4. As can be seen in Table 4.4, the exciplex free energy is roughly 0.3 eV lower for **ZnDHD6ee** coordinated by chloride or bromide ions than in the corresponding pure solvent. As shown in Figures 4.5 and 4.6, the absorption maximum of the CT band in the chloride- or bromide-coordinated dyad was shifted to the red by about 140 nm relative to that of the non-coordinated dyad.

The oscillator strength of the transition from the ground state to the exciplex was determined from the corresponding absorption spectrum using Equation 2.13 [56]. Because the CT absorption band overlaps partially with absorptions of the low energy transitions of porphyrin and fullerene chromophores, the fitted spectra of the CT bands (the blue curves in Figure 4.6) were used to calculate the oscillator strength of the transition in the region 7000-22000 cm^{-1} (see paper II for the details). The oscillator strengths in both the ligated and non-ligated dyads were relatively large (0.020-0.026, Table 4.4). It was found that the oscillator strength of the transition from the ground state to the exciplex is only 3 times lower than that of the ground state to the S_1

state in both the non-coordinating and coordinating environments. In addition, the halide binding resulted in an increase in the oscillator strength of the CT absorption band by ~15-20 % relative to that of the non-ligated one as can be seen in Table 4.4. The decrease in ΔG° and increase in the oscillator strength for the coordinated dyads were explained by the electric field generated by the negative charge of the halide ligated to the porphyrin ring on the side opposite to the fullerene and thus facilitating the electron density shift from the porphyrin to fullerene.

The electronic coupling matrix elements of the transition from the ground state to the exciplex of the dyad in both the non-ligating and ligating environments can also be estimated from the CT absorption band using Equation 2.12 [28,38,39]. It has been previously found that the electronic coupling for a series of double-linked porphyrin-fullerene dyads, including **ZnDHD6ee** depends on the center-to-center distance (R_{DA} in Equation 2.12) between the porphyrin and fullerene moieties [12]. All the spectral parameters in Equation 2.12 can be extracted from Figure 4.6, and the center-to-center distance can be estimated as ~7 Å as reported earlier [12,31]. The results of calculations are shown in Table 4.4.

Table 4.4. Energies obtained from the fitting of the absorption spectra of **ZnDHD6ee**, the calculated oscillator strengths, and the calculated electronic coupling matrix elements.

solvent/salt solution	ΔG° (eV)	λ_{rs} (eV)	V (cm^{-1})^{a}	f^{b}
Anisole	1.430	0.217	602	0.021
THF	1.389	0.221	586	0.020
PhCN	1.300	0.269	543	0.017
DMF	1.231	0.307	510	0.013
TBABr/anisole	1.119	0.285	647	0.026
TBACl/anisole	1.117	0.291	645	0.025
TBACl/THF	1.063	0.297	628	0.023

[a] Calculated from Equation 2.12. [b] Calculated from Equation 2.13.

As shown in Table 4.4, slightly stronger coupling (~10 %) is seen for **ZnDHD6ee** in the coordinating environment compared to the non-coordinating one, and the strongest coupling was observed for the bromide solution of anisole. This result is consistent with the obtained oscillator

strengths, since higher electronic coupling should lead to higher oscillator strength of the ground state to the exciplex transition. As stated above, the physical reason for the effect is the presence of the negative charge at the porphyrin side opposite to that of the fullerene, which facilitates the electron density shift from porphyrin to fullerene, i.e. lowers the energy of exciplex and makes the direct photo-excitation to the exciplex more efficient.

As shown in Section 4.3.1.1 (Figure 4.3b) the chloride binding to the central zinc of **ZnDHD6ee** resulted in an efficient quenching of the exciplex emission in the dyad and no emission band was detected in the red to near IR regions of the spectrum. Therefore, the emission decay of the exciplex could not be measured and its lifetime was not determined.

4.3.3 Anion ligand effect on the complete CS state

4.3.3.1 Zinc porphyrin-fullerene dyad

The oxidation and reduction potentials of **ZnDHD6ee** in non-coordinating and chloride-coordinating environments were determined by the DPV measurements and the resulting difference between these potentials were used to calculate the energy of the complete CS state of the dyad. The differential pulse voltammograms of **ZnDHD6ee** in both ligating and non-ligating solutions are shown in Figure 4.7.

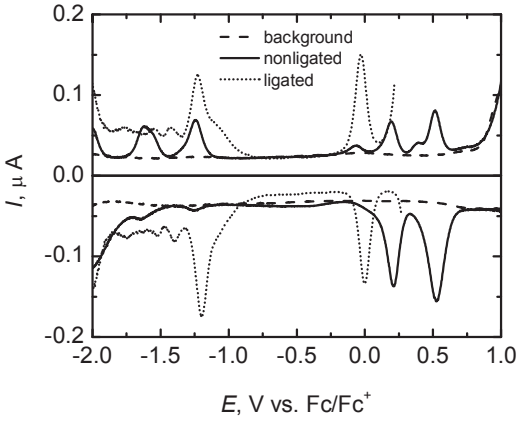

Figure 4.7. Differential pulse voltammograms of **ZnDHD6ee** in 0.1 M of $TBAPF_6/CH_2Cl_2$, and $TBACl/CH_2Cl_2$ solutions. The presented background is for $TBAPF_6/CH_2Cl_2$ solution. The potentials are expressed relative to the redox potentials of Fc/Fc^+, which were calculated from separate measurements with the same pseudo-reference electrode [I].

As can be observed in Figure 4.7, the chloride coordination leads to a lower oxidation potential of the ZnP moiety in **ZnDHD6ee**, similarly to the results reported earlier for zinc porphyrins [89]. The binding with chloride ion has only a minor effect on the reduction potential of the fullerene moiety, which is reasonable outcome as the ligation takes place between the chloride ion and the ZnP moiety. The difference in the first reduction potential of the fullerene moiety of the dyad in $TBAPF_6$ and TBACl solutions was only 40 mV, whereas the difference in the first oxidation potential of the ZnP moiety was 220 mV. Thus, the donor ability of the ZnP moiety of the dyad was enhanced by the coordination of chloride.

The energy of the complete CS state of the dyad was calculated (Equation 3.1, Section 3.3) considering the Coulombic attraction between the anion and cation [30]. Applying the center-to-center distance between the ZnP and fullerene moieties as ~7 Å [12,31] the complete CS state energies of **ZnDHD6ee** in $TBAPF_6/CH_2Cl_2$ and $TBACl/CH_2Cl_2$ were estimated roughly as 1.93 eV and 1.67 eV, respectively [paper I]. Thus, the chloride binding to the ZnP moiety of the dyad lowers the energy of both the exciplex and the complete CS state as can be expected.

The lifetime of the complete CS state was determined by measuring the absorption of the transient states of **ZnDHD6ee** with the pump-probe method (Section 3.4.1) using photo-excitation at ~ 405 nm. The transient absorption decay curves in a wide spectrum range were globally fitted using a three exponential model. The third component needed for the fitting of the experimental results had a lifetime too long to be resolved with the instrument. This component was found to arise from the solvents and not from the dyad itself (see paper I for the details), and that component was omitted from Figure 4.8 for clarity.

The decay component spectra for the non-coordinated and chloride-coordinated dyads are presented in Figure 4.8. The exciplex state in both the non-ligated and chloride-ligated dyads could not be observed directly in the pump-probe measurements, because the exciplex and the complete CS state have rather similar spectral features and close lifetimes [12]. The second component has features of both the exciplex and the complete CS state (Table 4.3). In these experiments the excitation populates the second singlet excited state of the porphyrin chromophore, which relaxes rapidly to the S_1 state and was not resolved in the measurements. The component with a 2.3 ps time constant (Figure 4.8a) for the non-ligated dyad is clearly too

long-lived to be assigned to the S_1 state of the ZnP chromophore in the dyad, as the lifetime of this state was found to be 0.5 ps in the up-conversion measurements (Section 4.3.1.1). As was discussed previously (Section 4.2) the equilibrium between the exciplex and the complete CS state is established in picosecond time domain, and since this process starts from the exciplex, establishing of the equilibrium means some rise of the population of the complete CS state. The rise of the complete CS state population is also confirmed by the negative (rise) intensities of the fast component at wavelengths specific for the complete CS state, around 650 and 860 nm.

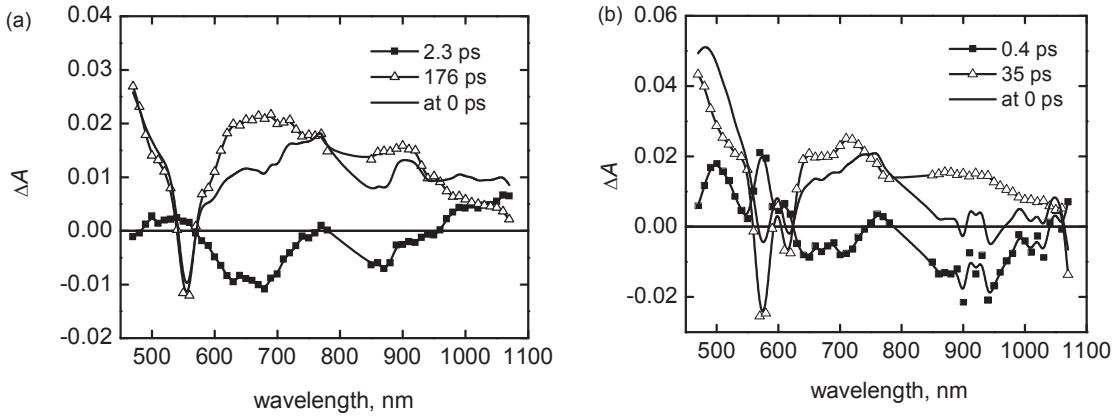

Figure 4.8. Transient absorption decay component spectra and calculated time-resolved spectra at 0 delay time for **ZnDHD6ee** in (a) anisole and (b) TBACl/anisole.

The second component with a 176 ps time constant shows clear spectral features of the ZnP radical cation at 600-750 nm [100], and fullerene radical anion around 800-1100 nm. As opposed to the sharp peak at ~1050 nm for the anion of pristine C_{60} [101], the broad anion band is characteristic for the doubly-linked fullerene [12,22,23]. For the non-ligated dyad in anisole, it was shown in Section 4.2 that the relaxation process to the ground state via the exciplex dominates (by ~ 91 %) over that via the complete CS state, because the exciplex energy is lower than that of the complete CS state and the population of the exciplex is higher than that of the complete CS state (Table 4.3). According to the mathematical analysis carried out for **ZnTBD6bee** in Section 4.2, the theoretical value of the time constant for direct relaxation of the CS state to the ground state in anisole is ~ 9 ns (Figure 4.2). This value is considerably larger than the experimentally observed lifetime in the pump-probe experiments (Figure 4.8), since in

anisole the population of the complete CS state is very small and if this state is formed it decays quickly via the intramolecular exciplex.

For the chloride-coordinated dyad, the shape of the second component was different compared to that in the non-coordinated dyads, and this component was assigned to the complete CS state (see paper I for detailed discussion). The lifetime of the second component in the chloride-ligated **ZnDHD6ee** (35 ps) was found to be even shorter than that observed for the dyad in polar benzonitrile (46 ps, Table 4.1).

Compared to the non-ligated **ZnTBD6ee** in anisole, the CR process was found to be ~260 times faster in the ligated dyad (Figures 4.2 and 4.8). The faster back ET of the chloride-ligated dyad is reasonable taking into account the increased donor ability of the ZnP moiety, which was observed as lowering of the first oxidation potential in the TBACl solution compared to that in the non-coordinated dyad (Figure 4.7). The shorter lifetime of the complete CS state for the ligated **ZnDHD6ee** is explained by the lower energy of the complete CS state compared to the non-ligated one. This result is consistent with the Marcus inverted region [25-29] for such compounds.

4.3.3.2 Zinc phthalocyanine-fullerene dyads

The first one-electron oxidation and reduction potentials of the ZnPc and fullerene moieties of **ZnPc-C_{60}ee** were determined with the DPV measurements (Section 3.3) of the ligated and non-ligated dyads in CH_2Cl_2. The differential pulse voltammograms in non-coordinating and chloride-coordinating environments are presented in Figure 4.9.

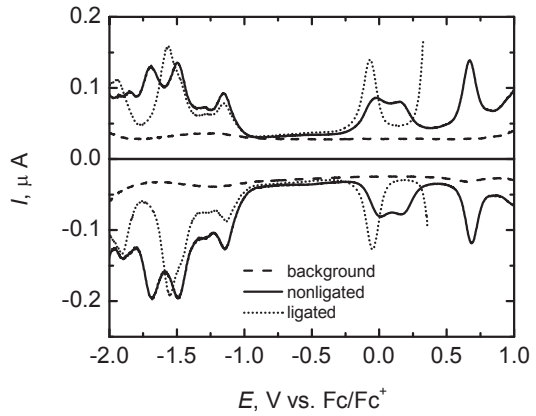

Figure 4.9. Differential pulse voltammograms of **ZnPc-C_{60}ee** in 0.1 M of $TBAPF_6/CH_2Cl_2$ (nonligated), and $TBACl/CH_2Cl_2$ (ligated) solutions. The presented background is for $TBAPF_6/CH_2Cl_2$ solution. The potentials are expressed relative to the redox potentials of Fc/Fc^+, which were measured separately using the same pseudo-reference electrode [paper I].

The reduction potential of fullerene was found to be the same for both the chloride-ligated and non-ligated dyads whereas the oxidation potential of ZnPc chromophore is lower than that of the non-ligated one by 70 mV (Section 4.4). The differences between E_{ox} and E_{red} (Equation 3.1) for the chloride-coordinated and non-coordinated **ZnPc-C_{60}ee** were 1.07 eV and 1.14 eV, respectively. The difference for the non-ligated dyad agrees very well with that reported previously for a similar double-linked zinc phthalocyanine-fullerene dyad in PhCN (1.16 eV) [23]. The energies of the CS state of the dyad in different ligating and non-ligating solutions were estimated from Equation 3.1 accounting for the Coulombic attraction between the anion and cation **[30]**. The CS state energies of the dyad in different coordinating and non-coordinating solutions were estimated applying the center-to-center distance between ZnPc and fullerene moieties to be 13 Å for the major extended conformation of **ZnPc-C_{60}ee** [22]. The decrease in the CS state energy in the coordinated dyads indicates that the axial ligation of the chloride to the ZnPc moiety enhances slightly the electron donor ability of ZnPc chromophore.

The absorption of the transient states were measured with the pump-probe technique using the photo-excitation at ~ 390 nm, and the absorption decay curves were globally fitted using a bi-exponential model. The shapes of decay component spectra for the dyad were found to be similar in all of the non-ligating and chloride-ligating environments (see Figure 4.10 for the dyad in DMF and its chloride complex as an example). In all cases the formation of the CS state after

relaxation of the locally excited S_1 state of ZnPc chromophore was seen. The components with 14 ps and 11 ps time constants for the non-ligating and chloride-ligating dyads, respectively, can be assigned to the decay of the CS state of the dyad (Figure 4.10). The characteristic absorption band of phthalocyanine radical cation was observed around 800-900 nm. The band is broadened compared to the band of the free radical cation of phthalocyanine [102], because of the interaction between the phthalocyanine cation and the fullerene anion in the dyad [22,23]. Similarly to double-linked porphyrin-fullerene dyads studied previously [12], and other phthalocyanine-fullerene dyads [22,23], it has been shown that the anion of the di-substituted fullerene gives rise to absorption in a broad spectral range, 900-1100 nm, instead of the sharp peak of the pristine fullerene anion at ~1050 nm [101]. The fastest component can be attributed to the transition from the S_1 state of ZnPc chromophore to the CS state.

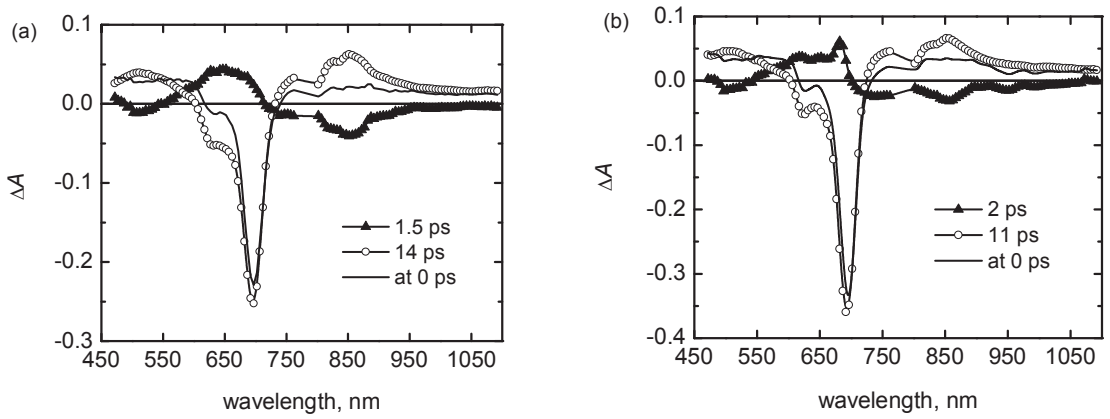

Figure 4.10. Transient absorption decay component spectra and calculated time-resolved spectra at 0 delay time for **ZnPc-C_{60}ee**: (a) in DMF and (b) in TBACl/DMF.

As shown in Figure 4.10, the CR process was slightly faster in the chloride-coordinated dyad. The chloride binding to the ZnPc moiety of **ZnPc-C_{60}ee** accelerated this process by almost 1.3 times. This effect is much weaker than the corresponding one observed on the CR process of the zinc porphyrin-fullerene dyad (Figure 4.8). The rate constants of the charge separation (CS) and CR processes in the dyad are discussed in the following section.

4.4 The inverted region behavior for the phthalocyanine-fullerene dyad

The conclusion of the Marcus inverted region behavior [25-29] for the electron transfer and back electron transfer reactions of the phthalocyanine-fullerene dyad (**ZnPc-C_{60}ee**) was drawn after studying the effect of the chloride binding with ZnPc moiety of the dyad on the ET reaction in a series of solvents (Table 4.6).

It was observed that decreasing the driving force of the CR process of **ZnPc-C_{60}ee** results in an increase in the rate constant of the reaction, k_{CR}, (Table 4.6). The energy of the CS state, i.e. the free energy of the CR process, is lower for the ligated dyad compared to the non-ligated one and the rate constant of this process is larger than that observed in the corresponding non-coordinating environment (Table 4.6). Similarly to the case for porphyrin-fullerene dyads [20,21,74], the Marcus inverted region phenomenon has been earlier established for the CR process for several covalently linked phthalocyanine-fullerene dyads [18,64].

Interestingly, the charge separation process is also located in the Marcus inverted region. The driving force of this process ($-\Delta G_{CS}$) in **ZnPc-C_{60}ee** was estimated as the difference between the energy of the first singlet excited state of zinc phthalocyanine (E_{ph}) and the energy of the complete CS state (ΔG_{cs}). The E_{ph} and ΔG_{cs} values were estimated from the steady absorption and emission, and from the DPV measurements, respectively. It is seen from Table 4.6 that the CS rate constant, k_{CS}, in all of the chloride-coordinated dyads is smaller when ΔG_{CS} becomes larger, which is also consistent with the Marcus inverted region behavior [25-29]. The charge separation process of **ZnPc-C_{60}ee** in all of the chloride-ligating solutions was 1.2-1.4 times slower than that in the corresponding non-ligating environments (Table 4.6). The slowing down of the forward ET rate constant upon the axial chloride binding to the central zinc of the dyad is in agreement with the steady state fluorescence measurements (Section 4.3.1.2), because the increase in the lifetime of S_1 state was also observed as an increase in the fluorescence intensity of the ligated **ZnPc-C_{60}ee** (Figure 4.4b). The inverted region behavior found for **ZnPc-C_{60}ee** differs from that for porphyrin-fullerene dyads reported several times, since in porphyrin-fullerene dyads, which have the extended conformation with long center-to-center distance between porphyrin and fullerene moieties, the charge separation process has been found to occur in the normal region of Marcus parabola [20,21,74].

Table 4.6. Rate constants of CS and CR processes, k_{CS} and k_{CR}, respectively, phthalocyanine singlet excited state and CS state energies, E_{ph} and ΔG_{cs}, respectively, the driving force of the CS reaction, ΔG_{CS}, and the reorganization energy, λ_r, for **ZnPc-C$_{60}$ee** in coordinating and non-coordinating environments.

solvent/salt solution	k_{CS} (s^{-1})[a]	k_{CR} (s^{-1})[a]	E_{ph} (eV)[b]	ΔG_{cs} (eV)[c]	ΔG_{CS} (eV)[d]
DMF	6.79×10^{11}	7.15×10^{10}	1.78	1.169	-0.611
TBACl/DMF	4.87×10^{11}	8.96×10^{10}	1.79	1.099	-0.691
PhCN	3.82×10^{11}	3.47×10^{10}	1.77	1.183	-0.587
TBACl/PhCN	2.74×10^{11}	4.61×10^{10}	1.78	1.113	-0.667
CH_2Cl_2	1.56×10^{11}	1.66×10^{10}	1.76	1.264	-0.496
TBACl/CH_2Cl_2	1.17×10^{11}	2.23×10^{10}	1.77	1.194	-0.576
anisole	9.46×10^{10}	8.88×10^{9}	1.75	1.396	-0.354
TBACl/anisole	7.29×10^{10}	1.14×10^{10}	1.76	1.326	-0.434

[a] From pump-probe. [b] From steady state absorption and fluorescence measurements. [c] Calculated from Equation 3.1. [d] $\Delta G_{CS} = -(E_{ph} - \Delta G_{cs})$.

As was shown in Section 2.1, in the classical Marcus theory of electron transfer the inverted region behavior means that the absolute value of the driving force must be larger than the reorganization energy [25-29]. For the dyad used in this study, the driving force was calculated to be -0.611 eV in strong polar solvents, such as DMF (Table 4.6), and reorganization energy must therefore be smaller than 0.61 eV. In an earlier study for a very similar dyad, the reorganization energy has been estimated based on the continuum theory [25-29], and assuming that R_{DA} is 12.5 Å, and $R_D = R_A = 4$ Å. The estimated reorganization energy of the CS process has been found to be 0.95 eV in PhCN [22], which is clearly larger than $-\Delta G_{CS}$. In frame of the obtained present results, this raises questions on the validity of the continuum model for that estimation and/or correctness of the parameters used for the estimation. For example, using R_{DA} = 10 Å, R_D = 6 Å and R_A = 4 Å, the reorganization energy will be 0.6 eV, which is just at the limit separating normal and inverted regimes of the charge separation for this dyad. Therefore, in this study the qualitative results of attributing the charge separation process to the Marcus inverted region are considered to be more reliable than the previous estimation based on a simple geometrical model of the dyad. The detailed discussion of the reorganization energy and driving

force for the CS process of **ZnPc-C_{60}ee**, and the difference between the cases for phthalocyanine- and porphyrin-fullerene dyads are presented in paper IV.

5 Conclusions

The following conclusions can be drawn based on the reported results:

1. A mathematical description of the equilibrium reaction and relaxation of the exciplex and the complete CS state in porphyrin-fullerene dyads was worked out to study quantitatively the intrinsic rate constants of the reactions and the energetic parameters they depend on. The mathematical model is based on the Marcus ET theory and the Boltzmann distribution, and it enables to separate the rate constants involved in synchronous relaxations of the exciplex and the complete CS state to the ground state. The developed model can be applied to calculate the free energies, the populations, the ET rate constants, and the direct relaxation rate constants of both the exciplex and the complete CS state to the ground state for such dyads at any value of the dielectric constant of the solvent. Thus, a clear discrimination is obtained between the two equilibrated intermediates, which have rather similar transient absorption spectra.
2. The energy balance between the exciplex and the complete CS state was found to occur in an environment with a solvent dielectric constant of 6.4. At this value the populations, the energies, and the rate constants of the equilibrium between the exciplex and the complete CS state become equal. In solvents with higher dielectric constants, the energy of the complete CS state is lower than that of the exciplex and the relaxation takes place via the complete CS state predominantly, whereas in solvents with lower polarities the energy of the complete CS state is higher and the exciplex relaxes directly to the ground state.
3. The analysis of the reaction rate constants suggests rather high electronic coupling between the exciplex and ground state, 0.25 eV. This finding corroborates the rather high oscillator strength for the transition from the ground state to the exciplex (the CT absorption band) for zinc porphyrin-fullerene dyads, which is only three times lower than that of the Q band of the zinc porphyrin chromophore.
4. The chloride coordination to a zinc porphyrin-fullerene dyad lowers the energies of both the exciplex and the complete CS state and accelerates the ET processes. Similarly, the

energy of the CS state is lower and recombination is faster upon chloride binding to a zinc phthalocyanine-fullerene dyad though the change is smaller than for the zinc porphyrin-fullerene dyad. These effects were explained by the electric field induced by the negative charge of the chloride ligated to the central metal. The electric field reduces the energy of the CS state, which leads to faster charge recombination due to the inverted Marcus regime of the back electron transfer reaction in both dyads.

5. The effect of anion ligation on the exciplex energy can be seen as a gradual red shift of the CT absorption band of the zinc porphyrin-fullerene dyad. Also the oscillator strength of the CT absorption band increases by 15-20 % upon the chloride ligation.

6. The chloride ligation to the zinc phthalocyanine moiety of the zinc phthalocyanine-fullerene dyad results in an increase in the driving force of the charge separation process, and a decrease in the ET rate constant. Thus also the forward ET reaction in this dyad was found to occur in the Marcus inverted region.

6 References

1. Ben-Shem, A.; Frolow, F.; Nelson, N. *Nature* **2003**, *426*, 630-635.
2. Gust, D.; Moore, T. A. *Science* **1989**, *244*, 35-41.
3. Meyer, T. J. *Acc. Chem. Res.* **1989**, *22*, 163-170.
4. Wasielewski, *Chem. Rev.***1992**, *92*, 435-461.
5. Gust, D.; Moore, T. A. Moore, A. L. *Acc. Chem. Res.* **2001**, *34*, 40-48.
6. Kuciauskas, D.; Liddell, P. A.; Lin, S.; Johnson, T. E.; Weghorn, S. J.; Lindsey, J. S.; Moore, A. L.; Moore, T. A.; Gust, D. *J. Am. Chem. Soc*. **1999**, *121*, 8604-8614.
7. Luo, C.; Guldi, D. M.; Imahori, H.; Tamaki, K.; Sakata, Y. *J. Am. Chem. Soc*. **2000**, *122*, 6535-6551.
8. Imahori, H.; Mori, Y.; Matano, Y. *J. Photochem. Photobiol.* C **2003**, *4*, 51-83.
9. Imahori, *Org. Biomol. Chem.* **2004**, *2*, 1425-1433.
10. Kuramochi, Y.; Sandanayaka, A. S. D.; Satake, A.; Araki, Y.; Ogawa, K.; Ito, O.; Kobuke, Y. *Chem. Eur. J.* **2009**, *15*, 2317-2327.
11. Gust, D.; Moore, T. A. Moore, A. L. *Acc. Chem. Res.* **1993**, *26*, 198-205.
12. Chukharev, V.; Tkachenko, N. V.; Efimov, A.; Guldi, D. M.; Hirsch, A.; Scheloske, M.; Lemmetyinen, H. *J. Phys. Chem. B* **2004**, *108*, 16377-16385.
13. D'Souza, F.; Ito, O. *Coord. Chem. Rev.* **2005**, *249*, 1410-1422.
14. Escosura, A. de la; Martinez-Diaz, V.; Guldi, D. M.; Torres, T. *J. Am. Chem. Soc*. **2006**, *128*, 4112-4118.
15. Imahori, H.; Hagiwara, K.; Akiyama, T.; Aoki, M.; Tanigushi, S.; Okada, T.; Shirakawa, M.; Sakata, Y. *Chem. Phys. Lett.* **1996**, *263*, 545-550.
16. Guldi, D. M.; Prato, M. *Acc. Chem. Res.* **2000**, *33,* 695-703.

17. Imahori, H.; Tkachenko, N. V.; Vehmanen, V.; Tamaki, K.; Lemmetyinen, H.; Sakata, Y.; Fukuzumi, S. *J. Phys. Chem. A* **2001**, *105*, 1750-1756.

18. Tkachenko, N. V.; Efimov, A.; Lemmetyinen, H. *J. Porphyrins Phthalocyanines* **2011***, 15,* 780-790.

19. Guldi, D. M.; Luo, C.; Prato, M.; Dietel, E.; Hirsch, A.; *Chem. Commun.* **2000**, 373-374.

20. Guldi, D. M.; Hirsch, A.; Scheloske, M.; Dietel, E.; Troisi, A.; Zerbetto, F.; Prato, M. *Chem. Eur. J.* **2003**, *9*, 4968-4979.

21. Schuster, D. I.; Cheng, P.; Jarowski, P. D.; Guldi, D. M.; Luo, C.; Echegoyen, L.; Pyo, S.; Holzwarth, A. R.; Braslavsky, S. E.; Williams, R. M.; Klihm, G. *J. Am. Chem. Soc*. **2004**, *126*, 7257-7270.

22. Isosomppi, M.; Tkachenko, N. V.; Efimov, A.; Vahasalo, H.; Jukola, J.; Vainiotalo, P.; Lemmetyinen, H. *Chem. Phys. Lett.* **2006**, *430*, 36-40.

23. Niemi, M.; Tkachenko, N. V.; Efimov, A.; Lehtivuori, H.; Ohkubo, K.; Fukuzumi, S.; Lemmetyinen, H. *J. Phys. Chem. A* **2008**, *112*, 6884-6892.

24. D'Souza, F.; Gadde, S.; Zandler, M. E.; Arkady, K.; El-Khouly, M. E.; Fujitsuka, M.; Ito, O. *J. Phys. Chem. A* **2002,** *106*, 12393-12404.

25. Marcus, R. A.; Sutin, N. *Biochim. Biophys. Acta* **1985**, *811*, 265-322.

26. Bolton, J. R.; Archer, M. D. *Adv. Chem. Ser.* **1991**, *228*, 7-23.

27. Gould, I. R.; Young, R. H.; Moody, R. E.; Farid, S. *J. Phys. Chem*. **1991**, *95*, 2068-2080.

28. Marcus, R. A. *Rev. Mod. Phys.* **1993**, *65*,599-610.

29. Barbara, P. F.; Meyer, T. J.; Ratner, M. A. *J. Phys. Chem.* **1996**, *100*, 13148-13168.

30. Kavarnos, G. J. "*Fundamentals of Photoinduced Electron Transfer*", VCH Publisher, Inc., New York, **1993**; pp 37-40.

31. Chukharev, V.; Tkachenko, N. V.; Efimov, A.; Lemmetyinen, H. *Chem. Phys. Lett.* **2005**, *411*, 501-505.

32. Murata, S.; Tachiya, M. *J. Phys. Chem. A* **2007**, *111*, 9240-9248.

33. Braslavsky, S. E. *Pure & Appl. Chem.* **2007**, *79*, 293-465.

34. Dresner, J.; Prochorow, J.; Ode, W. *J. Phys. Chem.* **1989**, *93*, 671-677.

35. Kuzmin, M. G. *Pure & Appl. Chem.* **1993**, *65*, 1653-1658.

36. Rathore, R.; Hubig, S. M.; Kochi, J. K. *J. Am. Chem. Soc*. **1997**, *119*, 11468-11480.

37. Mattes, S. L.; Farid, S. *Acc. Chem. Res.* **1982**, *15,* 80-86.

38. Gould, I. R.; Young, R. H.; Mueller, L. J.; Farid, S. *J. Am. Chem. Soc*. **1994**, *116*, 8176-8187.

39. Gould, I. R.; Young, R. H.; Mueller, L. J.; Albrecht, A. C.; Farid, S. *J. Am. Chem. Soc*. **1994**, *116*, 8188-8199.

40. Mataga, N.; Chosrowjan, H.; Taniguchi, S. *J. Photochem. Photobiol C.* **2005**, *6*, 37.

41. Kesti, T. J.; Tkachenko, N. V.; Vehmanen, V.; Yamada, H.; Imahori, H.; Fukuzumi, S.; Lemmetyinen, H. *J. Am. Chem. Soc*. **2002**, *124*, 8067-8077.

42. Isosomppi, M.; Tkachenko, N. V.; Efimov, A.; Lemmetyinen, H. *J. Phys. Chem. A* **2005**, *109*, 4881-4890.

43. Kuzmin, M. G.; Soboleva, I. V.; Dolotova, E. V. *J. Phys. Chem. A* **2007**, *111*, 206.

44. Lemmetyinen, H.; Tkachenko, N. V.; Efimov, A.; Niemi, M. *J. Phys. Chem. C* **2009**, *113*, 11475.

45. Mataga, N. *Pure & Appl. Chem.* **1993**, *65*, 1605-1610.

46. Tkachenko, N. V.; Lemmetyinen, H.; Sonoda, J.; Ohkubo, K.; Sato, T.; Imahori, H.; Fukuzumi, S. *J. Phys. Chem. A* **2003**, 107, 8834-8844.

47. Armaroli, N.; Marconi, G.; Echegoyen, L.; Bourgeois, J.-P.; Diederich, F. *Chem. Eur. J.* **2000**, *6*, 1629-1645.

48. Imahori, H.; Tkachenko, N. V.; Vehmanen, V.; Tamaki, K.; Lemmetyinen, H.; Sakata, Y.; Fukuzumi, S. *J. Phys. Chem. A* **2001**, *105*, 1750-1756.

49. Vehmanen, V.; Tkachenko, N. V.; Imahori, H.; Fukuzumi, S.; Lemmetyinen, H. *Spectrochim. Acta A* **2001**, *57*, 2229-2244.

50. D'Souza, F.; Maligaspe, E.; Karr, P. A.; Schumacher, A. L.; Ojaimi, M. E.; Gros, C. P.; Barbe, J.-M.; Ohkubo, K.; Fukuzumi, S. *Chem. Eur. J.* **2008**, *14*, 674-681.

51. Ruppert, M.; Spänig, F.; Wielopolski, M.; Jäger, C. M.; Bauer, W.; Clark, T.; Hirsch, A.; Guldi, D. M. *Chem. Eur. J.* **2010**, *16*, 10797-10807.

52. Marcus, R. A. *J. Phys. Chem.* **1989**, *93*, 3078-3086.

53. Gould, I. R.; Farid, S. *Acc. Chem. Res.* **1996**, *29,* 522-528.

54. Gould, I. R.; Young, R. H.; Mueller, L. J.; Albrecht, A. C.; Farid, S. *J. Am. Chem. Soc*. **1994**, *116*, 3147-3148.

55. Gould, I. R.; Noukakis, D.; Gomez-Jahn, L.; Goodman, J. L.; Farid, S. *J. Am. Chem. Soc*. **1993**, *115*, 4405-4406.

56. Turro, N. J. "*Modern Molecular Photochemistry*", The Benjamin/Cummings Publishing Company, Inc., California, **1978**, pp 86-88.

57. De Bolster, M. W. G.; Cammack, R.; Coucouvanis, D. N.; Reedijk, J.; Veeger, C. *Pure & Appl. Chem.* **1997**, *69*, 1251-1303.

58. Lo, P.-C.; Leng, X.; K.P.Ng, D. *Coord. Chem. Rev.* **2007**, 251, 2334-2353.

59. Antipas, A.; Gouterman, M. *J. Am. Chem. Soc.* **1983**, *105*, 4896.

60. Bendikov, M.; Wudl, F.; Perepichka, D. F. *Chem. Rev.* **2004**, *104,* 4891-4945.

61. Dorough, G. D.; Miller, J. R.; Huennekens, F. M. *J. Am. Chem. Soc*. **1951**, *73*, 4315-4320.

62. Starukhin, A.; Vogel, E.; Waluk, J. *J. Phys. Chem. A* **1998**, *102*, 9999-10006.

63. de la Torre, G.; Va´zquez, P.; Agullo´-Lo´pez, F.; Torres, T. *Chem. Rev.* **2004**, *104*, 3723-3750.

64. Bottari, G.; de la Torre, G.; Guldi, D. M.; Torres, T. *Chem. Rev.* **2010**, *110*, 6768-6816.

65. Kroto, H. W.; Heath, J. R.; O'Brien, S. C.; Curl, R. F.; Smalley, R. E. *Nature* **1985**, *318*, 162-163.

66. Krätschmer, W.; Lamb, L. D.; Fostiropoulos, K.; Huffman, D. R. *Nature* **1990**, *347*, 354-358.

67. Echegoyen, L.; Echegoyen, L. E.; *Acc. Chem. Res.* **1998**, *31*, 593-601.

68. Reed, C. A.; Bolskar, R. D. *Chem. Rev.* **2000**, *100,* 1075-1120.

69. Da Ros, T.; Prato, M.; Guldi, D. M.; Ruzzi, M.; Pasimeni, L. *Chem. Eur. J.* **2001**, *7*, 816-827.

70. Vail, S. A.; Schuster, D. I.; Guldi, D. M.; Isosomppi, M.; Tkachenko, N. V.; Lemmetyinen, H.; Palkar, A.; Echegoyen, L.; Chen, X.; Zhang, J. Z. H. *J. Phys. Chem. B*, **2006**, *110,* 14155-14166.

71. D'Souza, F.; Chitta, R.; Gadde, S.; Shafiqul Islam, D.-M.; Schumacher, A. L.; Zandler, M. E.; Araki, Y.; Ito, O. *J. Phys. Chem. B* **2006**, *110,* 25240-25250.

72. Schuster, D. I.; Li, K.; Guldi, D. M.; Palkar, A.; Echegoyen, L.; Stanisky, C.; Cross, R. J.; Niemi, M.; Tkachenko, N. V.; Lemmetyinen, H. *J. Am. Chem. Soc*. **2007**, *129*, 15973-15982.

73. Yamada, H.; Ohkubo, K.; Kuzuhara, D.; Takahashi, T.; Sandanayaka, A. S. D.; Okujima, T.; Ohara, K.; Ito, O.; Uno, H.; Ono, N.; Fukuzumi, S. *J. Phys. Chem. B* **2010**, *114*, 14717-14728.

74. Imahori, H.; Tamaki, K.; Guldi, D. M.; Luo, C.; Fujitsuka, M.; Ito, O.; Sakata, Y.; Fukuzumi, S. *J. Am. Chem. Soc*. **2001**, *123*, 2607-2617.

75. Scheidt, W. R.; Reed, C. A. *Chem. Rev.* **1981**, *81*, 543-555.

76. Momenteau, M.; Reed, C. A. *Chem. Rev.* **1994**, *94*, 659-698.

77. Antipas, A.; Gouterman, M. *J. Am. Chem. Soc.* **1983**, *105*, 4896.

78. Becker, R. S.; Allison, J. B. *J. Am. Chem. Soc.* **1963**, *67*, 2662-2669.

79. Becker, R. S.; Allison, J. B. *J. Am. Chem. Soc.* **1963**, *67*, 2669-2675.

80. Allison, J. B.; Becker, R. S. *J. Am. Chem. Soc.* **1963**, *67*, 2675-2679.

81. Davila, J.; Harriman, A.; Milgrom, L. R. *Chem. Phys. Lett.* **1987**, *136*, 427-430.

82. Holten, D.; Bocian, D. F.; Lindsey, J. S. *Acc. Chem. Res.* **2002**, *35*, 57-69.

83. Campbel, W. M.; Burrell, A. K.; Officer, D. L.; Jolley, K. W. *Coord. Chem. Rev.* **2004**, *248*, 1363-1379.

84. Miller, J. R.; Dorough, G. D. *J. Am. Chem. Soc.***1952**, *74*, 3977-3981.

85. Kirksey, C. H.; Hambright, P.; Storm, C. B. *Inorg. Chem.* **1969**, *8*, 2141.

86. Kadish, K. M.; Shiue, L. R.; Rhodes, R. K.; Bottomley, L. A. *Inorg. Chem.* **1981**, *20*, 1274-1277.

87. Seki, H.; Hoshino, M.; Shizuka, H. *J. Phys. Chem*. **1989**, *93*, 3630-3634.

88. Gust, D.; Moore, T. A.; Moore, A. L. Kang, H. K.; DeGraziano, J. M.; Liddell, P. A.; Seely, G. R. *J. Phys. Chem*. **1993**, *97*, 13637-13642.

89. Seely, G. R.; Gust, D.; Moore, T. A.; Moore, A. L. *J. Phys. Chem.* **1994,** *98*, 10659-10664.

90. Nappa, M.; Valentine, J. S. *J. Am. Chem. Soc*. **1978**, *100*, 5075-5080.

91. Hutchison, J. A.; Sintic, P. J.; Brotherhood, P. R.; Scholes, C.; Blake, I. M.; Ghiggino, K. P.; Crossley, M. J. *J. Phys. Chem. C* **2009**, *113*, 11796-11804.

92. Guldi, D. M.; Zilbermann, I.; Gouloumis, A.; Va´zquez, P.; Torres, T. *J. Phys. Chem. B* **2004**, *108*, 18485-18494.

93. Efimov, A.; Vainiotalo, P.; Tkachenko, N. V.; Lemmetyinen, H. *J. Porphyrins Phthalocyanines* **2003***, 7,* 593-599.

94. Zewail, A. H. *J. Phys. Chem. A* **2000**, *104*, 5660-5694.

95. Tkachenko, N. V. "*Optical Spectroscopy Methods and Instrumentations*" Elsevier, Amsterdam, **2006**.

96. Niemi, M., "*Photoinduced Electron Transfer in Dyads and Triads of Porphyrins, Phthalocyanines, and Fullerenes*", Doctoral Thesis, Tampere University of Technology, Publication 732, Tampere, **2008**.

97. Stokkum, I. H. M. V.; Larsen, D. S.; Grondelle, R. V. *Biochim. Biophys. Acta* **2004**, *1657*, 82-104.

98. Arnold, B. R.; Noukakis, D.; Farid, S.; Goodman, J. L.; Gould, I. R. *J. Am. Chem. Soc*. **1995**, *117*, 4399-4400.

99. Arnold, B. R.; Farid, S.; Goodman, J. L.; Gould, I. R. *J. Am. Chem. Soc*. **1996**, *118*, 5482-5483.

100. Gasyna, Z.; Browett, W. R.; Stillman, M. J. *Inorg. Chem.* **1985**, *24*, 2440-2447.

101. Greaney, M. A.; Gorun, S. M. *J. Phys. Chem.* **1991,** *95*, 7142-7144.

102. Nojiri, T.; Alam, M. M.; Konami, H.; Watanabe, A.; Ito, O.; *J. Phys. Chem. A* **1997**,*101*, 7943.

Tampereen teknillinen yliopisto
PL 527
33101 Tampere

Tampere University of Technology
P.O.B. 527
FI-33101 Tampere, Finland

ISBN 978-952-15-3077-7
ISSN 1459-2045